Photon- and electron-induced fission at intermediate energies

V. G. Nedorezov

Institute of Nuclear Research, USSR Academy of Sciences, Moscow

Yu. N. Ranyuk

Physico-Technical Institute, Ukrainian Academy of Sciences, Khar'kov

Fiz. Elem. Chastits At. Yadra **15**, 379–417 (March–April 1984)

Photon- and electron-induced fission of nuclei at energies from the pion-production threshold to several giga-electron-volts is reviewed. Data on the cross sections of photon- and electron-induced fission in the region of giant resonances and the region corresponding to the quasideuteron mechanism of photoabsorption are also discussed. The virtual-photon method, which is used to analyze experimental data, is described in the distorted-wave Born approximation and in the plane-wave Born approximation with allowance for the nuclear sizes. Data on the energy, mass, and angular distributions of the fragments of photon- and electron-induced fission are analyzed in a wide range of excitation energies. Data on the dependence of the fissility of nuclei with $Z \leqslant 83$ on the parameter Z^2/A are systematized. The mechanisms of photon- and electron-induced fission at intermediate energies are discussed.

INTRODUCTION

Investigations of fission at excitation energies appreciably exceeding the fission barrier of the actinide nuclei have developed strongly in recent years. The interest in them is due primarily to the possibility of obtaining information about fundamental nuclear properties manifested in cascade meson–nucleon and nucleon–nucleon processes, the fission and fragmentation of relatively light nuclei, the production of hypernuclei, etc. The investigation of nuclear reactions and, in particular, fission serves in this case as a tool for solving problems encountered in high-energy physics. Among them we can mention questions of the relationship between exchange currents and the problem of quark bags, which arise in the study of electrodisintegration of the deuteron or quasideuteron, in the measurement of the quadrupole moment of the Δ (1232) isobar in photo- and electroproduction of pions, and so forth. At the same time, there are possibilities for obtaining new information about the influence of a nuclear medium on the nature of elementary processes. A good example is provided by the differences observed in the cross sections of total photodisintegration on free deuterons and on quasideuterons in nuclei, in the pion photoproduction cross sections on nucleons and nuclei, and so forth.

It should be noted that the development of high-energy nuclear physics was also stimulated by the need to solve important applied problems associated with the radiative strength of materials, the creation of intense neutron sources, the development of radiation biology, medicine, etc.

Among the investigations in high-energy nuclear physics, those in which nuclei are excited by electrons, positrons, and photons occupy an important position. To a large degree this is the case because, as a rule, the electromagnetic interactions of nuclei can be described in the framework of simpler models than nucleon–nucleus collisions, and therefore the interpretation of the data in the former case is simpler.

In this review, we shall largely restrict ourselves to the range of electron and γ energies that is now usually referred to as the intermediate range,[1] namely, from the pion-production threshold to several giga-electron-volts. But we shall also consider data on photo- and electrofission of nuclei at low energies, which are needed to describe the observed effects in the considerd region. It should be noted that in reactions induced by bremsstrahlung photons and high-energy electrons an important part is played by processes with low momentum transfer, leading to low excitation energies of the nuclei. The reason for this is that the spectrum of bremsstrahlung and virtual photons is continuous.

The first experimental data on electron-induced fission apeared at the end of the sixties, but for a long time the main attraction was devoted to photonuclear reactions, including photofission. There are by now a number of reviews[2–4] that systematize the results of photo- and electrofission investigations at intermediate energies. However, they do not cover the large amount of data, primarily on electrofission published in recent years.

It is interesting to note that whereas the development of photonuclear investigations followed the traditional path in the direction of ever higher energies, the first electrofission studies were begun at energies above 100 MeV.[5–7]

1. ASPECTS OF FISSION INDUCED BY PHOTONS, ELECTRONS, AND POSITRONS. THE VIRTUAL-PHOTON METHOD

The fission of nuclei at intermediate and high energies is influenced by the entire nuclear-excitation mechanism preceding the fission. Therefore, experimental data on fission cross sections and on the angular and energy distributions of the fragments can be used not only to study the fission itself (measure the height of the barrier, the level density at the saddle point, etc.) but also to obtain information about the paramters of the original interaction (excitation energies, the number of cascade nucleons, and so forth). This aspect of fission at high excitation energies is manifested especially clearly in the case of nuclei with $Z = 90$, for which the fissility approaches unity when $E_\gamma \gtrsim 20$ MeV, which made it possible, by measurement of the photofission cross section, to obtain data on the total cross sections of photoabsorption.[8] Moreover, the cause of high-energy particles made it

 0090-4759/84/020172-18$04.40

possible to bring into the ambit of fission physics almost the entire periodic table, which provided new possibilities for testing different nuclear models and fission mechanisms.

The main difficulty in the study of photonuclear and electronuclear reactions is that the spectrum of bremsstrahlung and virtual photons is continuous, so that processes in the entire energy range—from the threshold to the upper limit of the spectrum $[(E_e - m_e)$, where E_e and m_e are the total and rest mass of the electron (positron)]—contribute to the experimentally measured reaction yield. Work on the creation and use of beams of monoenergetic photons has only just begun (in the region of intermediate energies), and their contribution to the study of photofission is as yet very small (see below).

According to the virtual-photon method,[9] the electron–nucleus interaction can be represented in the form of the simple diagram

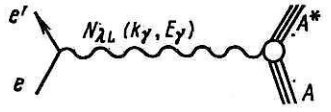

Besides the purely electromagnetic vertex [$\hat{A}_\nu(k_\gamma, E_\gamma$ is the Møller potential for the scattered electron), the interaction Hamiltonian contains the matrix element of the current operator $J_\nu(k_\gamma, E_\gamma)$ for the system $A \to A^*$:

$$H(k_\gamma, E_\gamma) = \sum_\nu \hat{A}_\nu(k_\gamma, E_\gamma) J_\nu(k_\gamma, E_\gamma), \quad (1)$$

where κ_γ is the momentum transfer, and E_γ the energy transfer.

The electrofission cross section σ_{ef} and the photofission yield per equivalent photo, σ_{Qf}, are related to the photofission cross section $\sigma_{\gamma f}$ by

$$\sigma_{ef}(E_e) = \sum_{\lambda L} \int_0^{E_e - m_e} N_{\lambda L}(E_e, E_\gamma)\, \sigma_{\gamma f}(E_\gamma)\, dE_\gamma / E_\gamma; \quad (2)$$

$$\sigma_{Qf}(E_e) = \sum_{\lambda L} \int_0^{E_e - m_e} N(E_e, E_\gamma)\, \sigma_{\gamma f}(E_\gamma)\, dE_\gamma / E_\gamma. \quad (3)$$

Here, $N_{\lambda L}(E_e, E_\gamma)$ is the spectrum of the virtual photons, which depends in the general case on the multipolarity L of the interaction, and also on the mass of nucleus A, its charge, and radius; λ is the electric or magnetic transition. The photofission cross section is represented as a multipole expansion:

$$\sigma_{\gamma f}(E_\gamma) = \sum_{\lambda L} \sigma_{\lambda L}(E_\gamma). \quad (4)$$

The virtual photons have both transverse and longitudinal polarization, and therefore the summation in (2) for the electric multipole fields begins with zero, and not unity, as in (3) for the photons.

Typical arrangements of experiments to study photo- and electronuclear reactions at intermediate energies are shown in Fig. 1.

It should be noted that if γ bremsstrahlung is used the spectrum $N(E_e, E_\gamma)$ can be measured experimentally. This spectrum is determined by the conditions of formation of the

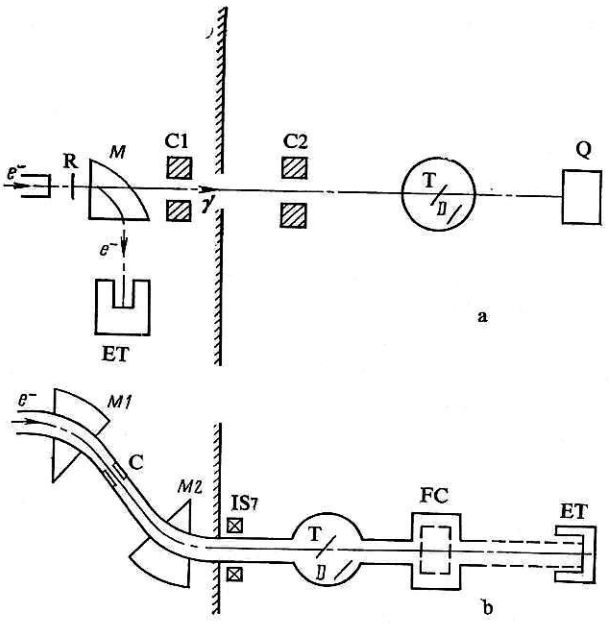

FIG. 1. Typical arrangement of experiments to study nuclear reactions induced by photons (a) and electrons (b). M1 and M2 are analyzing magnets, and M is a sweeping magnet; C, C_1, and C_2 are collimators; IS is the beam-intensity sensor (magnetoinduction, secondary emission, etc.); T is the target; D is the detector of the reaction products (fission fragments); FC is a Faraday cup (shown with a broken line, since it is usually removed from the beam in the measurements); R is the radiator; Q is the quantameter; and ET is an electron trap.

photon beam and does not depend on the investigated nucleus. In contrast, the virtual-photon spectrum is determined by the properties of the target nucleus and the natue of the investigated reaction. Therefore, the analysis of electrofission results, which are more informative than photofission data, is much more complicated.

From the methodological point of view, the use of electrons (virtual photons) has a number of definite advantages compared with real bremsstrahlung photons. If one is working with a photon beam, only part of the bremsstrahlung produced in the radiator is cut out by the collimators, and because of the energy dependence of the cross section of multiple electron scattering the intensity and spectral composition of the bremsstrahlung beam incident on the investigated target can vary strongly with the energy of the electrons and depend on the quality of the guiding of the beam in the accelerator. By exposing the target directly to electrons, one can have a constant flux of virtual photons virtually independent of the electron energy. If an electron beam is used, the problems of focusing and monitoring the beam are more readily solved.

At the same time, it should be noted that the cross section of electron-induced reactions is approximately two orders of magnitude lower than that of photonuclear reactions, so that the electron beam must satisfy more stringent requirements with regard to the various backgrounds, above all photons and neutrons. The electron beam must be formed in such a way as to reduce to a minimum the concomitant γ radiation produced in the collimators, chamber walls, and so forth. For this, one uses parallel transport of the electron

beam, and the scattering chamber is connected directly to the vacuum electron guide of the accelerator. In addition, scattering of the electrons by the target leads to appreciable radiative backgrounds, which present difficulties for the detecting apparatus.

In this connection, much attention is currently being paid to the creation of beams of quasimonoenergetic and tagged photons. However, the intensities of the beams obtained by annihilation of accelerated positrons as well as of beams of tagged photons are as yet very low and require the use of thick targets. Therefore, at the present time such beams are used mainly to study photoneutron reactions, and it is only recently that such investigations have advanced into the region of energies above the giant resonance to the pion-production threshold.[10] Fission data were then obtained by analyzing the photoneutron yields. Direct measurements of the photofission cross section of ^{238}U induced by quasimonoenergetic photons based on detection of the fission fragments were made in the experiment described in Ref. 11 (at $E_\gamma = 11.5$ MeV). For the region of intermediate energies, there are results of investigation of the ^{238}U fission cross section by means of quasimonoenergetic photons from a diamond crystal.[12]

2. SPECTRUM OF BREMSSTRAHLUNG AND VIRTUAL PHOTONS

The bremsstrahlung spectrum from a thin target, when the electron ionization losses can be ignored, was calculated by Schiff[13] and has frequently been described in the literature devoted to the calculation of cross sections from yield curves based on solution on the integral equations (2). Among the numerous methods of cross-section calculation we may mention the methods of Penfold and Leiss,[14] Cook,[15] and Thies.[16] At γ energies above 100 MeV, Schiff's spectrum has a form close to $N \sim 1/E$, and Eq. (2) can be readily solved analytically:

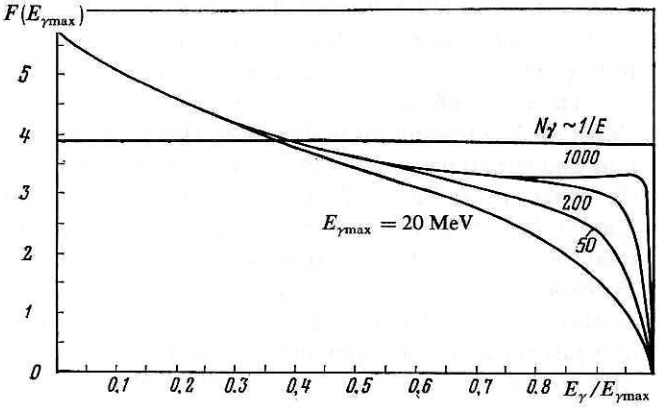

FIG. 2. Bremsstrahlung flux for different $E_{\gamma max}$.

$$\sigma_{\gamma f}(E_\gamma) = d\sigma_{Qf}(E_e)/d\ln E_e. \tag{5}$$

Figure 2 shows the γ fluxes $F = \int N(E_e, E_\gamma)dE_\gamma$ for different E_e, from which it can be seen that with increasing E_e the F distribution gets closer to a right angle. The errors in the calculation of $\sigma_{\gamma f}$ from the yield curves are analyzed in Ref. 17, where it is shown that the expression (5) can be used with an error of 10–15% at energies above 100 MeV.

In contrast to the bremsstrahlung spectrum, the virtual-photon spectrum cannot be directly measured in an experiment, and its calculation is a rather difficult problem. The virtual-photon spectrum is determined by inelastic electron-scattering processes and in the plane-wave Born approximation (PWBA) for an infinitely heavy nucleus has the form[9]

$$N_{\lambda L}(E_e, E_\gamma) = N^t_{\lambda L}(E_e, E_\gamma) + N^l_{\lambda L}(E_e, E_\gamma), \tag{6}$$

where $N^t_{\lambda L}$ and $N^l_{\lambda L}$ are the terms of the spectrum with transverse and longitudinal polarization of the photons, respectively:

$$N^t_{\lambda L}(E_e, E_\gamma) = \frac{\alpha}{4\pi}\int\limits_{(p_e-p_{e'})^2}^{(p_e+p_{e'})^2} \frac{[(p_e-p_{e'})^2-k_\gamma^2]\,[k_\gamma^2-(p_e-p_{e'})^2+2k_\gamma^2\,(k_\gamma^2-E_\gamma)^2]}{(k_\gamma^2-E_\gamma^2)^2} \left(\frac{k_\gamma}{E_\gamma}\right)^{2L} \frac{B(\lambda L,\ k_\gamma)}{B(\lambda L,\ E_\gamma)}\, d(k_\gamma^2); \tag{7}$$

$$N^l_{\lambda L}(E_e, E_\gamma) = \frac{\alpha}{2\pi}\int\limits_{(p_e-p_{e'})^2}^{(p_e+p_{e'})^2} \frac{L}{(L+1)\,p_e^2} \frac{(p_e+p_{e'})^2-k_\gamma^2}{k_\gamma^2} \left(\frac{k_\gamma}{E_\gamma}\right)^{2L-2} \frac{B(CL,\ k_\gamma)}{B(\lambda L,\ E_\gamma)}\, d(k_\gamma^2), \tag{8}$$

where p_e and $p_{e'}$ are the momenta of the initial and scattered electron, $k_\gamma = p_e - p_{e'}$, $E_\gamma = E_e - E_{e'}$, and B are structure functions, which will be discussed below.

In the long-wavelength approximation ($k_\gamma R \ll 1$, where R is the nuclear radius), when the nucleus can be regarded as a point, the structure functions become constant, and Eq. (6) can be integrated analytically. The virtual-photon spectra for a point nucleus have frequently been calculated for electric and magnetic transitions of all multipolarities.[17,18] Expressions for these spectra are given in a convenient form in Barber's paper[18]:

$$N_{\lambda L}(E_e, E_\gamma) = \frac{\alpha}{\pi}\frac{1}{E_\gamma}\left\{\left[1+\left(\frac{E_e-E_\gamma}{E_e}\right)^2\right] \times \ln\frac{2E_e(E_e-m_e)}{m_e E_\gamma} - C_L\right\}. \tag{9}$$

where α is the fine-structure constant, $C_L = 2(E_e - E_\gamma)/E_e$ for $\lambda L = E1$ (electric dipole transition), $C_L = 0$ for $\lambda L = M1$, and

$$C_L = -\frac{8}{3}[(E_e - E_\gamma)/E_e]^2$$

for $\lambda L = E2$. It can be seen that the difference between the spectra due to the multipolarity of the interaction decreases

with increasing electron energy.

The PWBA cannot be regarded as satisfactory, since it does not reflect the dependence of the intensity of the virtual photons on the charge of the nucleus and does not take into account the distortions of the electron wave function in the nuclear Coulomb field. The problem of the Coulomb corrections to the virtual-photon spectrum was first considered in Refs. 19–21. The most correct expression was obtained by Gargaro and Onley[21] using the distorted-wave Born approximation (DWBA) as a result of expanding the electron and positron wave functions with respect to a basis of Dirac Coulomb functions. The nucleus was assumed to have a point charge. The resulting spectrum has the form

$$N_{\lambda L}(E_e, E_\gamma) = \frac{\alpha}{\pi}\frac{p_e^2 k_\gamma^4}{2L+1}\Sigma S(L)(2J_1+1)(2J_2+1) \times \left| C\left(J_1 J_2 \lambda L, -\frac{1}{2}\frac{1}{2}\right) R^2(K, L, K_\gamma)\right|^2, \quad (10)$$

where $S(L)$ is the operator that ensures fulfillment of the selection rules for the electric and magnetic multipoles, R is the integral of the product of radial solutions of the Coulomb Dirac equation and the radial part of the electromagnetic Green's function, and C are Clebsch–Gordan coefficients.

The expression (10) is rather complicated for numerical calculations. Such calculations and their results are described in Refs. 22 and 23. In accordance with Ref. 22, the expressions for the virtual-photon spectrum for the $E1$ transition can be represented in the form

$$N_{E1}^{-}(E_e, E_\gamma, Z) = N_{E1}^{PW}(E_e, E_\gamma) + E_\gamma[1.29\cdot 10^{-5}\exp(1.245Z^{1/3} - 0.052E_e)]E_e'/E_e \quad (11)$$

for electrons and

$$N_{E1}^{+}(E_e, E_\gamma, Z) = N_{E1}^{PW}(E_e, E_\gamma) - 3\cdot 10^{-5}\exp(0.675Z^{1/3} - 0.06135E_e)E_e' \quad (12)$$

for positrons. Here, N_{E1}^{PW} is the virtual-photon spectrum for the $E1$ transition in the plane-wave approximation, E_e, $E_e' \geqslant m_e$, $E_e' > 0.405\exp(0.206Z^{1/2})$.

Since electrons are attracted by the nucleus, and positrons repelled, the amplitude of the electron wave function near the nucleus is larger than the amplitude of the positron wave function at the same energy. Since all the remaining aspects of the interaction of the electron and positron with the nucleus are the same, the number of virtual photons associated with electron scattering by the nucleus is higher than in the case of positrons.

The first distorted-wave Born approximation is entirely adequate for the interpretation of the experimental data in the region of the giant resonance if a limitation is made to an error of about 10% (for the heaviest nuclei). As can be seen from Eqs. (11) and (12), the Coulomb corrections decrease strongly with increasing E_e and decreasing Z. At $E_e \gtrsim 100$ MeV, their value does not exceed 1–2%.

To obtain a higher accuracy in calculations of the virtual-photon spectra it is necessary to take into account the nuclear structure. The first-order corrections taking into account the nuclear size were first considered by Barber[24] by exanding the electron wave function in powers of $k_{\gamma R}$. To take into account the nuclear structure, Shotter[25] used the general Helm model,[26,27] which proved itself well in the description of inelastic electron scattering. These calculations did not take into account the interaction of the nuclear magnetic moment with the electric field of the electron, i.e., magnetic transitions were not considered. In accordance with the generalized Helm model, the ratio of the structure functions [see Eq. (6)] has the form

$$\frac{B(E\lambda, k_\gamma)}{B(E\lambda, E_\gamma)} = \left(\frac{E_\gamma}{k_\gamma}\right)^{2(L+1)}\frac{j_L^2(k_\gamma R)}{j_L^2(E_\gamma R)}\exp[-g^2(k_\gamma^2 - E_\gamma^2)];$$
$$\frac{B(C\lambda, k_\gamma)}{B(E\lambda, E_\gamma)} = \left(\frac{E_\gamma}{k_\gamma}\right)^{2L}\frac{j_L^2(k_\gamma R)}{j_L^2(E_\gamma R)}\exp[-g^2(k_\gamma^2 - E_\gamma^2)]. \quad (13)$$

Here, j is a Bessel function, and g is a parameter characterizing the thickness of the surface layer of the nucleus, which in Shotter's calculations was taken equal to 0 and 1 F.

The main problem in using these equations for the region of intermediate energies is that the form factors in them give divergences already at energies E_γ above 120 MeV. To smooth the diffraction minima in the form factor, the squares of the spherical Bessel function were replaced in Ref. 28 by the expressions

$$j_L(k_\gamma R) \to \frac{j_L(k_\gamma+\varepsilon, R)+j_L(k_\gamma-\varepsilon, R)}{2}; \quad (14)$$
$$j_L(E_j, R) \to \frac{j_L(E_\gamma+\varepsilon, R)+j_L(E_\gamma-\varepsilon, R)}{2}.$$

The value of ε was taken to be 0.1, which in the case of nuclei with $A \sim 240$ corresponds to averaging over the energy with an interval of about 2 MeV. This procedure somewhat distorts the energy dependence of the form factor and makes it possible to avoid divergences.

We illustrate the above by examples. Figure 3 shows the virtual-photon spectra for the $E1$ excitation, calculated in the PWBA and with allowance for the Coulomb corrections for electrons and positrons with energy 20 MeV for a point nucleus ($Z = 92$). It can be seen in Fig. 4 that the Coulomb corrections to the virtual-photon spectrum decrease with increasing energy of the electrons (positrons) and for $E_e \geqslant 100$ MeV become negligibly small. The influence of allowance for the penetration of the electron wave function into the nucleus (allowance for the nuclear size) is shown in Fig. 5, which gives the virtual-photon spectra for $E1$ and $E2$ excitations, calculated for a point nucleus (continuous curves) and for a nucleus of finite size (broken curves) with mass

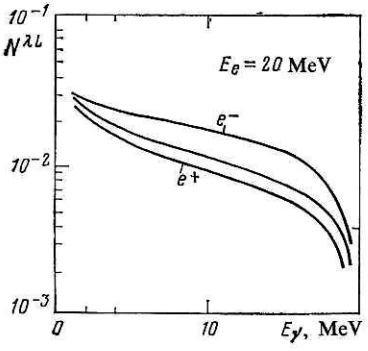

FIG. 3. Virtual-photon spectrum for $E1$ emission for 20-MeV electrons (or positrons), calculated in accordance with Eqs. (11) and (12) for $Z = 92$. The central curve is obtained without allowance for the Coulomb effects.

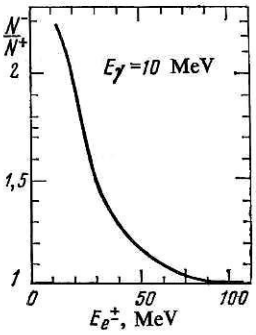

FIG. 4. Ratio of the number of virtual photons with energy 10 MeV obtained for scattering by uranium nuclei of electrons (N_{E1}^-) and positrons (N_{E1}^+) with initial energy 100 MeV.

$A = 238$. It can be seen that allowance for the form factor appreciably reduces the intensity of the virtual-photon spectrum, particularly for the $E2$ excitation. Despite this, the intensity of the quadrupole component in the spectrum is appreciably higher than that of the dipole component.

A general conclusion can be drawn on the basis of the above: At electron energy below 100 MeV, it is necessary to take into account the Coulomb corrections in calculating the virtual-photon spectra; at higher energies, it is important to take into account the nuclear size. At the same time, it must be borne in mind that the electron–nucleus interaction may be due to the quasideuteron or single-nucleon mechanism. The question of the form factor that must be taken into account in each specific case is as yet open.

Calculations of the spectra for the description of the (γ, d) reaction were made by Bethe and Peierls,[29] who took into account only $E1$ transitions. Pion electroproduction on free nucleons was analyzed by Dalitz and Yennie,[9] who considered $E1$, $E2$, and $M1$ interactions and took into account the influence of the nucleon size on $N_{\lambda L}$.

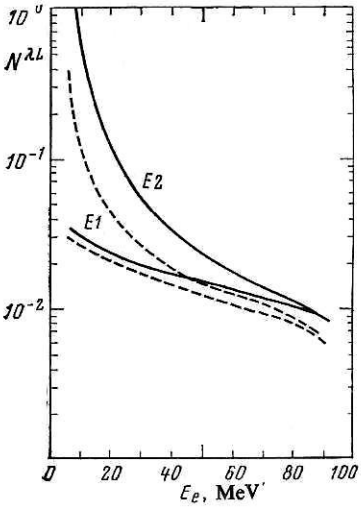

FIG. 5. Virtual-photon spectra for $E1$ and $E2$ emission without (continuous curves) and with (broken curves) allowance for the nuclear size, calculated in accordance with Eqs. (7) and (13) for 100-MeV electrons without allowance for the Coulomb effects for the uranium nucleus.

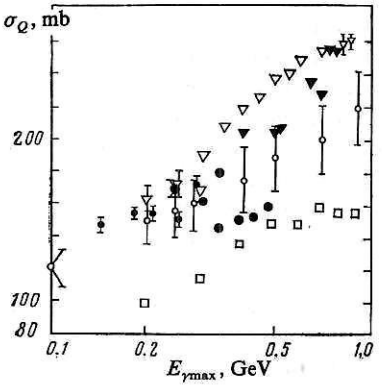

FIG. 6. Yield of the photofission reaction for ^{238}U as a function of the upper limit of the bresmsstrahlung spectrum. The open squares are the data from Ref. 30, the black circles from Ref. 35, the open triangles from Ref. 31, the black triangles from Ref. 32, and the open circles from Ref. 36.

3. PHOTOFISSION. YIELDS AND CROSS SECTIONS

In measurements with a bremsstrahlung beam, the yield of the photonuclear reaction is normalized by the flux of γ energy passing through the sample and detected by means of ionization chambers of quantameters. Thus,

$$\sigma_Q = \frac{\int_0^{E_e - m_e} N(E_e, E_\gamma)\,\sigma_\gamma(E_\gamma)\,dE_\gamma/E_\gamma}{\int_0^{E_e - m_e} N(E_e, E_\gamma)\,dE_\gamma}. \qquad (15)$$

Here, $N(E_e, E_\lambda)dE_\gamma$ is the number of photons in the energy interval E_γ–$(E_\gamma + dE_\gamma)$, and $E_e - m_e = E_{\gamma\,\max}$ is the limit of the bremsstrahlung spectrum. The cross section $\sigma_\gamma(E_\gamma)$ is determined from σ_Q by the methods indicated above.

The experimental data currently available on photofission cross sections at intermediate energies can be divided into two regions: $Z \geqslant 90$ and $Z \leqslant 83$.

In the region of intermediate energies, the photofission yield per equivalent photon, σ_{Q_f}, for nuclei in the region $Z \geqslant 90$ has been measured for ^{232}Th (Refs. 30–39), ^{235}U (Ref. 37), ^{238}U (Refs. 30–40), and also for the isotopes ^{241}Am and ^{243}Am (Ref. 8); there are also data on the relative yields for ^{236}U, ^{237}Np, and ^{239}Pu.[40] The largest number of investigations have been made with ^{238}U (Fig. 6). Note the large spread of yields obtained in the different laboratories. The discrepancy, which can be characterized by a factor 2, can, in particular, be explained by the presence of variations in the form of the bremsstrahlung spectrum at low energies and, because of this difference, in the contributions of the giant resonance to the total yield. At energies $E_{\gamma\,\max} = 100$ MeV, the contribution from the $E1$ resonance to the photofission yield is about 80%; for $E_{\gamma\,\max} = 1000$ MeV it reaches about 50%.[8]

At higher energies, data on the photofission yield are available only for ^{232}Th and ^{238}U up to $E_{\gamma\,\max} \simeq 6$ GeV (Fig. 7). As can be seen from Fig. 7, the characteristic feature of the energy dependence of the yield is the monotonic growth of σ_{Qf} with increasing $E_{\gamma\,\max}$.

For moderately heavy nuclei ($Z \leqslant 83$) the yields obtained in different laboratories agree to within the errors, as can be

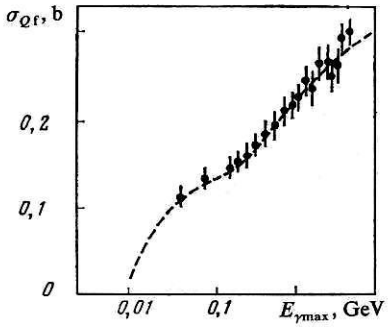

FIG. 7. The ^{238}U photofission yield in the range of $E_{\gamma max}$ from about 0.1 to 7 GeV.[36]

seen for the example of the nuclei Bi and Pb (Fig. 8). For nuclei with $Z \leqslant 83$, the photofission reaction threshold lies above the giant dipole resonance, and this to a large degree determines the higher accuracy of the measurements despite the relatively small cross sections in this region of energies.

Energy Dependence of Photofission Cross Sections

The cross sections $\sigma_{\gamma f}(E_\gamma)$ have been calculated from the yield curves for nuclei with $Z \geqslant 90$ by various authors, mainly for the nucleus ^{238}U (Refs. 30–36); see Fig. 9. Almost all solutions have a resonance nature (Refs. 30, 31, and 33–36); in Refs. 30 and 33–36, two maxima were found, at $E_\gamma = 300$ and 600 MeV; only in Ref. 32 is the cross section constant.

In the recently published paper of Ref. 11 the ^{238}U photofission cross section was determined using a beam of quasimonoenergetic photons produced by passing electrons through a diamond single crystal. These data are also shown in Fig. 9. The energy dependence of the cross section hardly differs from that of the majority of curves obtained with a bremsstrahlung beam, and the absolute values of the cross sections also agree on the average.

The least studied region of energies in nuclear photofission is the region from about 20 MeV to the pion-production threshold. Some points with fairly large errors were obtained for ^{241}Am and ^{243}Am (Fig. 10) in Refs. 8 and 28. Figure 10 also shows the data of measurements of the total photoabsorption cross sections for lead,[10] obtained using quasimonoenergetic photons with a correction for NA/Z in accordance with the sum rule. It is only at energies below 20 MeV, in the region of the giant dipole resonance, that the photofission cross section $\sigma_{\gamma f}$ and total photoabsorption cross section σ_{tot} can be regarded as known with sufficiently good accuracy. The most reliable data were obtained using beams of quasimonoenergetic photons for ^{238}U and ^{237}Np in Ref. 42 and for ^{238}U and ^{239}Pu in Ref. 43 (Fig. 11).

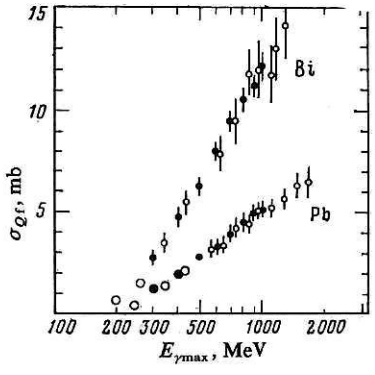

FIG. 8. The photofission yield for Bi and Pb. The open circles are the data from Ref. 60, and the black circles from Ref. 59.

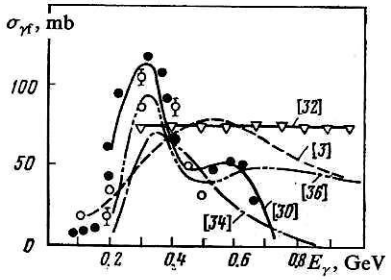

FIG. 9. The ^{238}U photofission cross section as a function of the photon energy. The black circles are the data from Ref. 11, the open triangles from Ref. 32, and the open circles represent a calculation in accordance with the cascade model.[1] (Literature sources are indicated by square brackets.)

The experimentally observed energy dependence of the photofission cross sections from 10 to 1000 MeV can be qualitatively explained in the framework of the currently adopted ideas about the mechanism of photon interaction with nuclei and nuclear fission. Figure 12 shows the curves of σ_{tot} and σ_f for ^{238}U calculated in accordance with these ideas (see below).

In the region of the giant dipole resonance, the cross section $\sigma_{\gamma f}$ can be represented as the sum of two Lorentz curves:

$$\sigma_{\gamma f} = D_f \sigma_{\text{tot}} = D_f \left[\frac{\sigma_{\parallel}}{\left(\frac{\omega^2 - \omega_{\parallel}^2}{\omega \Gamma_{\parallel}} \right)^2 + 1} + \frac{\sigma_{\perp}}{\left(\frac{\omega^2 - \omega_{\perp}^2}{\omega \Gamma_{\perp}} \right)^2 + 1} \right]. \tag{16}$$

Here, $\omega_{\parallel}$ and $\omega_{\perp}$ are the frequencies, $\sigma_{\parallel}$ and $\sigma_{\perp}$ the amplitudes, and $\Gamma_{\parallel}$ and $\Gamma_{\perp}$ the half-widths of the longitudinal and transverse resonances, and D_f is the fissility of the nucleus. Relations of the type (16), which are confirmed experimentally for a wide range of nuclei, follow from almost all the existing models of the giant dipole resonance and have a common nature.[44]

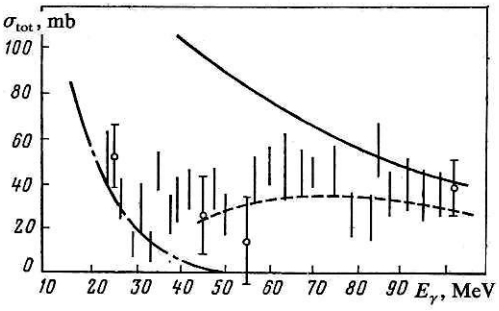

FIG. 10. Photofission cross sections averaged for the ^{241}Am and ^{243}Am nuclei.[8,28] The thin vertical lines show the cross sections of total photoabsorption obtained in Ref. 10 for Pb, multiplied by $(NZ/A)_{\text{Am}}/(NZ/A)_{\text{Pb}}$; the continuous curve is calculated in accordance with the quasideuteron model; the broken curve with allowance for the Pauli principle; and the chain curve shows the tail of the $E1$ giant resonance [calculation in accordance with Eq. (16)].

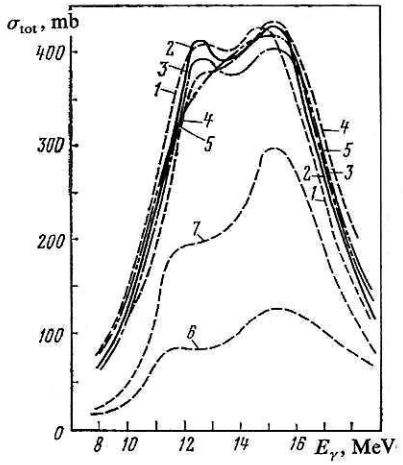

FIG. 11. Cross sections for total absorption of photons by nulcei: 1) ^{235}U; 2) ^{238}U (Ref. 42); 3) ^{238}U (Ref. 43); 4) ^{237}Np (Ref. 42); 5) ^{239}Pu (Ref. 43).

The cross sections corresponding to the absorption of photons with multipolarity higher than $E1$ make up a small part of the total cross section ($\sim 3\%$) and therefore can be effectively ignored. Some data on the quadrupole component obtained by analyzing the electrofission cross sections are discussed below.

In the region of energies up to the meson-production threshold, beginning with $E_\gamma \sim 50$ MeV, the photoabsorption cross sections can be satisfactorily described by means of the modified model of Levinger[45] [quasideuteron (qd) mechanism of photoabsorption]:

$$\sigma_{tot} \equiv \sigma_{qd} = L \frac{NZ}{A} \sigma_{\gamma d} e^{-S/E_\gamma}, \qquad (17)$$

where L, the Levinger constant, is calculated in Refs. 46 and 47 ($L \sim 10$ for $A \sim 240$); $\sigma_{\gamma d}$ is the photodisintegration cross section of the free deuteron[48]; and $S = 60$ MeV is a parameter introduced to take into account the suppression of the cross section in accordance with the Pauli principle at low momentum transfers (below the Fermi limit). Allowance for the Pauli principle has the consequence that the cross section is transformed from a rapidly decreasing exponential into a nearly constant cross section equal approximately to 30 mb (see Fig. 10).

Recently, good agreement between the calculations of σ_{qd} and experiments was obtained by Laget (Ref. 1, p. 275) on the basis of a model that takes into account the exchange

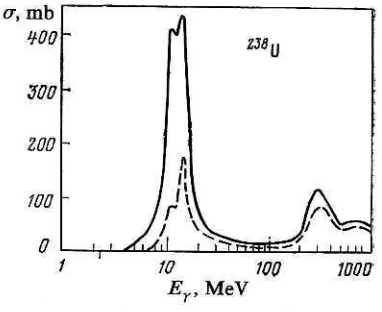

FIG. 12. Energy dependence of the total hadron cross section for photoabsorption for ^{238}U (continuous curve) and of the photofission cross section (broken curve), calculated in accordance with Eqs. (16)–(18).

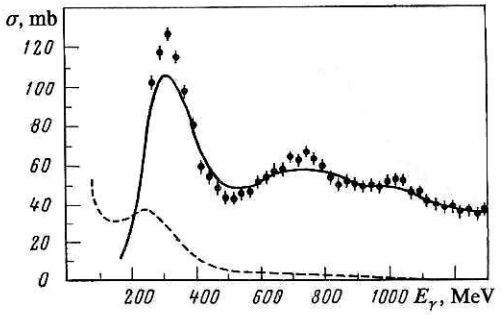

FIG. 13. Total hadron photoabsorption cross section $\sigma_{\gamma p}$ (Ref. 49), multiplied by $A = 241$ (points) and averaged over the momentum distribution of the nucleons in the nucleus (continuous curve). The broken curve is the cross section calculated in accordance with the quasideuteron model.

part of the cross section $\sigma_{\gamma d}$. The constant L, determined by comparison of theory and experiment, was found to be $L = 11 \pm 2$ for both light and heavy nuclei. Closer examination of the question of the value of L (A) is obviously of great interest from both the theoretical and experimental points of view.

At energies above the meson-production threshold, the cross section σ_{tot} is usually taken equal to the sum of the cross sections of pion photoproduction on the nucleons of the nucleus (averaged over the momentum distribution of the nucleons in the nucleus):

$$\sigma_{tot} = A\bar{\sigma}_{\gamma p}. \qquad (18)$$

Figure 13 shows the experimental points of Ref. 49, through which the smoothed curve $A\bar{\sigma}_{\gamma p}$ is drawn. the broken curve also shows the cross section σ_{qd} calculated using the quasideuteron mode.[45]

A dependence of the photofission cross sections on the photon energy similar to the one shown in Fig. 12 also holds for other nuclei, except that for nuclei with $Z \leqslant 83$ the peak corresponding to fission at the giant dipole resonance is absent. The continuous curve in Fig. 14 for the ^{209}Bi nucleus is obtained in accordance with the relation (3) with average (over the complete given energy interval) fissility $\bar{D}_f = 0.11$.

Fissilities and Absolute Values of the Cross Sections

Whereas the shape of the curves of the photoabsorption cross sections and the similar photofission cross sections (for

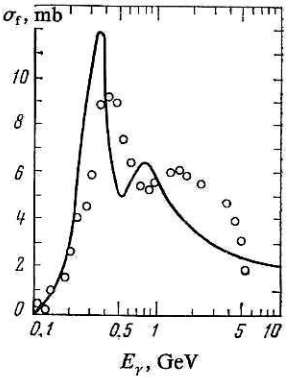

FIG. 14. Photofission cross section for bismuth nuclei. The points are obtained by solving Eq. (3) using the yields given in Ref. 36. The curve is explained in the text.

heavy nuclei) can be satisfactorily described in a wide range of energies—from the fission threshold to 1000 MeV—the dependence of the fissility on the excitation energy has been well studied only in the region of $E1$ giant resonance. It has been shown that for a number of nuclei with $Z \geqslant 90$ the fissilities can be well described by

$$D_f = \frac{\Gamma_f}{\Gamma_n + \Gamma_f} + \frac{\Gamma_n}{\Gamma_n + \Gamma_f} \frac{\Gamma'_f}{\Gamma'_n + \Gamma'_f} + \dots, \quad (19)$$

where the ratio of the neutron, Γ_n, and fission, Γ_f, widths ($\Gamma_{n,f}$ and $\Gamma'_{n,f}$ are the widths for the initial nucleus and for the nucleus formed after neutron emission) remains constant to excitation energies of order 40 MeV.[50] The fissilities increase by jumps as the excitation energy exceeds the energy of binding of the neutron to the residual nucleus. In the case of transuranium nuclei, which have a high initial fissility [for E_γ below the threshold of the (γ, nf) reaction] already when $E_\gamma \geqslant 20$ MeV, i.e., after emission of two or three neutrons, the fissilities becomes effectively equal to unity, but for ^{238}U ($\Gamma_f/\Gamma_n + \Gamma_f \sim 0.20$) and for nuclei with even smaller Z^2/A they continue to increase weakly. At energies $E_\gamma > 100$ MeV, fission is preceded by an intranuclear cascade and the statistical model [Eq. (19)] becomes invalid.

Calculations of the mean excitation energies in accordance with the cascade model were made in Refs. 51 and 52. In accordance with these calculations, the average numbers of cascade neutrons ($\Delta n_n \sim 3$) and protons ($\Delta n_p \sim 1.5$) depend weakly on the γ energy in the angle $100 < E_\gamma < 1000$ MeV for nuclei with $Z \geqslant 90$. Experimentally, the influence of the intranuclear cascade on the fission process has been little studied. It is probable that in the case of nuclei with a low fission barrier the emission of a small number of cascade protons hardly affects the fissibility, and it remains close to unity. For ^{238}U, ^{232}Th, and lighter nuclei the emission of even one proton may appreciably reduce the fissility. Experimental data on the fissility of nuclei with $Z \geqslant 90$ at intermediate energies are given in Ref. 40 (for ^{238}U, ^{237}Np, and ^{239}Pu, ^{241}Am, and ^{243}Am) (see also the reviews of Refs. 2–4).

Assuming that the photofission cross sections of the nuclei ^{241}Am and ^{243}Am are equal to the total photoabsorption cross sections in the region of energies above the pion-production threshold, Vinogradov *et al.*[8] obtained an unexpected result, namely, σ_{tot} exceeds by a factor of approximately 1.5 the sum of the cross sections of pion photoproduction on nucleons ($A\bar{\sigma}_{\gamma p}$). (The error in the measurement of the integrated cross section was about 15%). Other data on the total photoabsorption cross sections for heavy nuclei in this region of energies are as yet unavailable.

It should be noted that the adopted values $\sigma_{tot} = A\bar{\sigma}_{\gamma p}$ are undoubtedly only an estimate, since they ignore interference effects, nucleon correlation at short distances, etc., which may begin to play an important part on the transition to heavy nuclei. It is possible that part of the quasideuteron cross section σ_{qd} or the disintegration cross section of heavier clusters is added to the total cross section. The question of the contribution of fragmentation to the photodisintegration cross section of heavy nuclei remains open.

The experimental data on σ_{tot} for lighter nuclei are also quite insufficient. According to Ref. 53, the values of σ_{tot} in the region of the P_{33} resonance for Al, Ni, Mo, and W nuclei exceed by 30% the theoretical values. These data were obtained from electron-scattering experiments by extrapolating the measured inelastic-scattering cross section to the zero point as a function of the momentum transfer, σ_{ee},($q^2 \to 0$), and also need to be determined more accurately. The data obtained for the lightest nuclei (Li, Be) show that σ_{tot} is $\sim 80\%$ of $A\bar{\sigma}_{\gamma p}$ (see, for example, the papers of Arends *et al.* in Ref. 1).

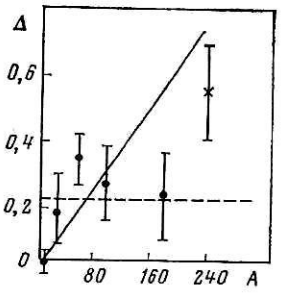

FIG. 15. The quantity $\Delta = (A\bar{\sigma}_{\gamma p} + C\bar{\sigma}_{\gamma\pi}/A\bar{\sigma}_{\gamma p}) - 1$ calculated in accordance with a model that takes into account the contribution of meson exchange currents.[54] The continuous line corresponds to $C \sim A^2$, and the broken line to $C \sim A$. The experimental data are taken from Ref. 53 (black circles) and Ref. 8 (cross).

As was noted in Ref. 54, the increase in the total photoabsorption cross section in the region of the baryon resonances could be due to the contribution of meson exchange currents. For E_γ above the pion-production threshold, the total cross section may contain besides the term $A\bar{\sigma}_{\gamma p}$ a correction $C\bar{\alpha}_{\gamma\pi}$, where C characterizes the number of pions in the nucleus, and $\bar{\sigma}_{\gamma\pi}$ is the cross section for total absorption of photons by nuclear pions, averaged over the momentum distribution of the pions in the nucleus. If it is assumed that the number of exchange pions is proportional to the number of nucleon pairs in the nucleus [$C = A(A-1)/2$], then even at comparatively small $\bar{\sigma}_{\gamma\pi} \sim 0.01\bar{\sigma}_{\gamma p}$ the exchange currents may make a contribution of $\sim 50\%$ for heavy nuclei (Fig. 15). The clarification of this question both experimentally and theoretically is important for understanding the interaction of photons with nuclei at energies corresponding to the baryon resonances.

Study of the fissility of heavy and moderately heavy nuclei as a function of Z^2/A is of great interest. This is due to the paper of Nix and Sassi,[55] who predicted a minimum of the fissility as a function of Z^2/A in the region of $A \sim 108$, and to the experimental discovery of an anomaly in this dependence for rare-earth nuclei.[56,57] From the methodological point of view, measurement of the fissilities of nuclei with $Z \leqslant 83$, which have small photofission cross sections, is rather difficult.

The experimental data so far obtained are shown in part in Fig. 16, from which it can be noted that the fissilities obtained in experiments with photons, protons, and α particles in the region $Z^2/A \geqslant 25$ are approximately the same but for $Z^2/A < 25$ differ rather strongly.

Analyzing the method used to determine the photofission yield, it is easy to note some deficiencies. First, in the experiments of Refs. 58 and 59 thick targets were used, the thickness exceeding the range of the fragments. The detec-

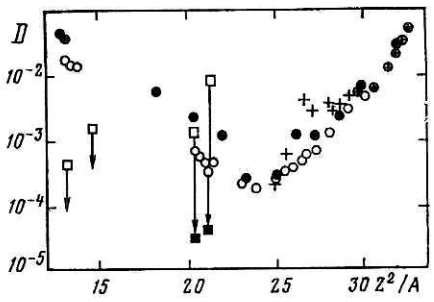

FIG. 16. Fissility as a function of the parameter Z^2/A, measured in experiments with photons (black circles, Ref. 30), protons (open circles, Ref. 56), and α particles (plus signs, open squares, and black squares, from Refs. 61 and 62).

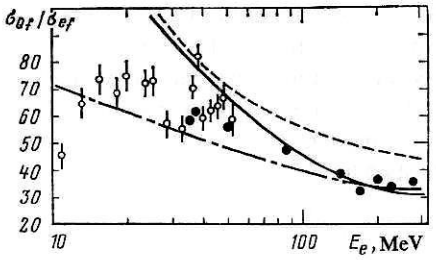

FIG. 17. Ratio of the photofission yield to the electrofission cross sections for the ^{238}U nucleus. The experimental data are taken from Ref. 30 (open circles) and Ref. 60 (black circles). The continuous curve is calculated in accordance with the expression (22); the broken curve, in accordance with Helm's generalized model with allowance for the nuclear structure.[26,27]

tors, glass in the given case, were placed right next to the surface of the target and, therefore, were irradiated by the beam. With decreasing mass of the fissioning nucleus, the photofission cross section and the fragment energy decrease. In this situation it becomes possible to detect not only fragments but other products of the nuclear reaction—recoil nuclei, nuclear fragments, and so forth. Therefore, the existence of a minimum in the Z^2/A dependence of the fissility cannot be regarded as proved.

We now turn to the region of the rare-earth nuclei ($Z^2/A = 25$–28). In Refs. 56 and 57, an irregularity was found in the dependence of the fissility on Z^2/A, this taking the form of a large value of the fission cross section of the heavy rare-earth elements compared with the predictions of the liquid-drop and cascade-evaporation model. The anomaly in the fission of the rare-earth nuclei is evidently a reflection of the irregularity in the fission barriers due to the deformation of these nuclei, i.e., ultimately shell effects, which must be taken into account correctly in calculations.

Thus, in the investigation of the Z^2/A dependence of the fissility there are two unresolved problems: the existence of an anomaly in the region of the rare earths (in Refs. 58 and 59, this anomaly was not noted) and the increase in the fissility with decreasing Z^2/A for nuclei lighter than silver. It is here necessary to make additional and more careful investigations.

Hitherto, we have assumed that at intermediate energies the fissility does not depend on the photon energy and we have given averaged valued. The determination of this dependence is hindered by the absence of reliable data on the total cross sections of nuclear photoabsorption and on the photofission cross sections. In recent experiments with quasimonoenergetic photons obtained using a diamond crystal the dependence of the fissility on the photon energy was measured for the ^{238}U nucleus,[12] and it was shown that there is a weak growth of the fissility with increasing photon energy.

4. RELATIONSHIP BETWEEN THE CROSS SECTIONS OF PHOTOFISSION AND ELECTROFISSION

The yield of a photonuclear reaction from a target bombarded with electrons can be represented as the sum of the contributions of the electro- and photonuclear reactions:

$$\left.\begin{aligned} Y(E_e,\ \Delta t) &= \sigma_e + \sigma_Q \Delta t; \\ \Delta t &= n_Q. \end{aligned}\right\} \tag{20}$$

Here, Δt is the electron bremsstrahlung mean freepath expressed in radiation units, and n_Q is the number of equivalent photons [Eq. (20) is valid if the bremsstrahlung path is short compared with the radiation unit ($\Delta t \ll 1$)].

Usually, the contributions of the photo-and electronuclear reactions are separated by measuring the reaction yield as a function of the thickness of the radiator. In the simplest case, two measurements are sufficient—one with and one without the radiator. Then

$$\frac{\sigma_Q}{\sigma_e} = \frac{Y_1 - Y_2}{\Delta t Y_2}, \tag{21}$$

where Y_1 is the reaction yield with the radiator, and Y_2 is the yield without it. In (20), the thickness of the target is ignored for simplicity.

Figure 17 represents the available experimental data on the energy dependence of σ_{Qf}/σ_{ef} for the uranium fission reaction. It can be seen that the ratio σ_{Qf}/σ_{ef} decreases slowly with increasing electron energy from 75 at $E_e = 20$ MeV to 35 at $E_e = 300$ MeV. The two upper curves in Fig. 17 were obtained by calculation in accordance with Eqs. (2) and (3); the continuous curve was obtained in accordance with the spectrum $N_{\lambda L}(E_e, E_\gamma)$ calculated in the PWBA without allowance for the nuclear structure, and the broken curve was obtained in accordance with Helm's generalized model (for $E1$ excitation of the nucleus). We should also mention the dependence most frequently used to express the connection between the photofission and electrofission cross sections[3] (the chain curve in Fig. 17):

$$\frac{\sigma_{Qf}}{\sigma_{ef}} = \frac{\pi}{2\alpha \ln E_e/m_e}, \quad \alpha = \frac{1}{137}. \tag{22}$$

This is obtained under the assumption of the $E1$ photoabsorption mechanism and under the condition that the effective γ energy satisfies

$$E_\gamma^{\text{эфф}} = \frac{\int E_\gamma \sigma_{\gamma f}(E_\gamma)\, N(E_e,\ E_\gamma)\, dE_\gamma/E_\gamma}{\int \sigma_{\gamma f}(E_\gamma)\, N(E_e,\ E_\gamma)\, dE_\gamma/E_\gamma} \ll E_e. \tag{23}$$

The last condition means that the contribution to the measured yield is determined mainly by processes with low energy transfer compared with the initial electron energy.

5. RATIO OF CROSS SECTIONS OF ELECTRON- AND POSITRON-INDUCED FISSION

Measurement of the ratio of the cross sections for fission induced by electrons (σ^-) and by positrons (σ^+) is one of the main experimental ways of testing the virtual-photon method. Figure 18 shows the values of σ^-/σ^+ obtained for the uranium and thorium fission reactions.[64,75] For $E_e \geqslant 100$ MeV, the ratio σ^-/σ^+ is near unity, which confirms the conclusion drawn earlier that the influence of Coulomb effects on the electron–nucleus interaction process becomes slight as the energy increases.

It can also be seen from Fig. 18 that the dependence σ^-/σ^+ is periodic, as was pointed out in Ref. 64. The oscillations with period of about 8 MeV were explained as follows. Since the ratio σ^-/σ^+ depends on the multipolarity of the excitation, and $\sigma(E2) > \sigma(E1)$, the oscillations indicate that with increasing energy of the electron (or positron) the relationship between the contributions of the $E1$ and $E2$ excitations to the fission changes periodically. In the general case, the $E1$ transition is predominant, but at low excitation energies the quadrupole transition may be predominant. This can happen if the low probability of $E2$ excitation is compensated by a higher probability of fission through the 2^+ fission barrier, which is lower than the 1^- barrier. The nucleus may have a low excitation energy not only near the fission threshold but also at the points corresponding to the evaporation of one, two, etc., neutrons.

It can be seen from Fig. 18 that on the average the σ^-/σ^+ ratios are well described by the DWBA calculation. This

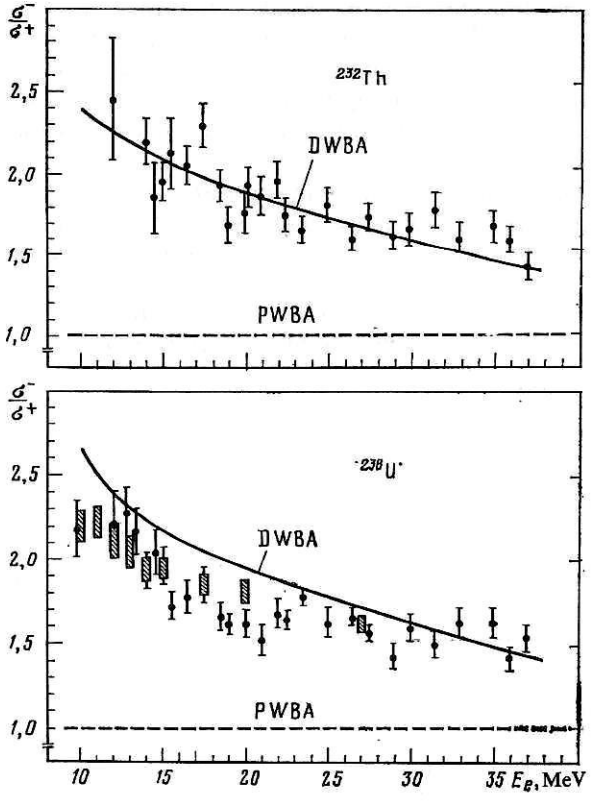

FIG. 18. Ratio of electron- and positron-induced fission cross sections for ^{232}Th and ^{238}U nuclei.[75]

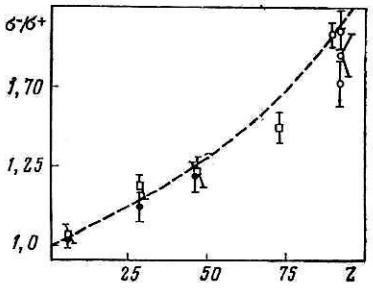

FIG. 19. Dependence of σ^-/σ^+ on the charge of the nucleus: open circles from Ref. 66, open squares from Ref. 67, and black circles from Ref. 68.

theory also gives a good description of the experimental data on the dependence of σ^-/σ^+ on the nuclear charge (Fig. 19).

6. ELECTROFISSION CROSS SECTION

The energy dependence of the electrofission cross sections is close to the dependence of the yield of the photofission reaction on the maximal energy of the bremsstrahlung spectrum [in the first approximation, it differs by the logarithmic factor $(\pi/2\alpha)\ln(E_e/m_e)$ (22)].

At low energies, detailed investigations of σ_{ef} were made by Arrudo Neto *et al.*[69,70] Figure 20 shows the ^{238}U

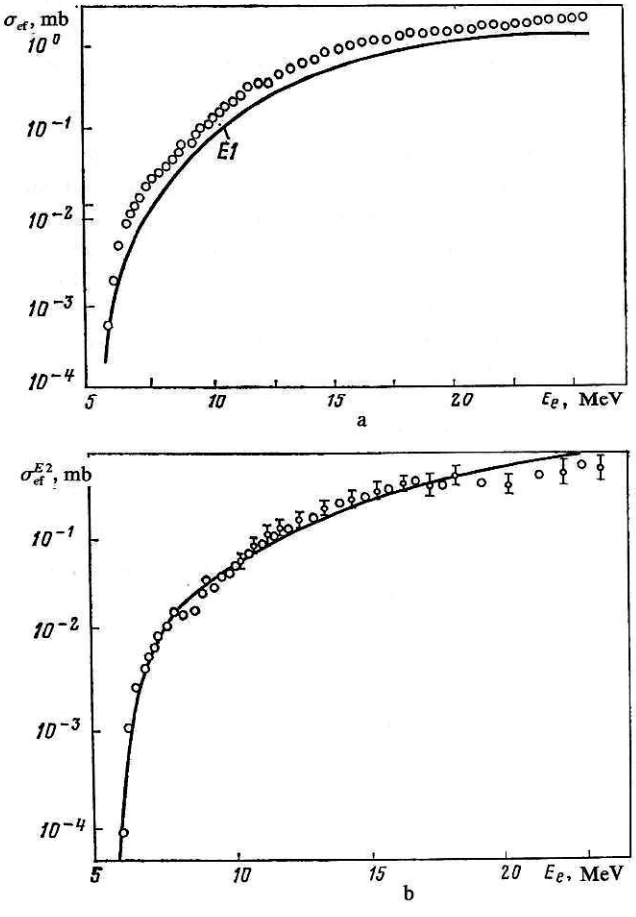

FIG. 20. Electrofission cross section for the ^{238}U nucleus (the curve is the calculation of σ_{ef}^{E1} in accordance with Eq. (2)) (a) and $\sigma_{ef}^{E2} = \sigma_{ef}^{exp} - \sigma_e^{E1}$ (Ref. 70) (b).

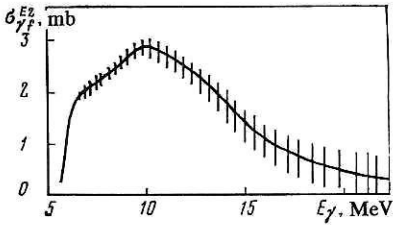

FIG. 21. THE ^{238}U photofission cross section in the region of the isoscalar quadrupole resonance.[70]

electrofission cross section and the difference between the measured experimental points and the calculated curve:

$$\sigma_{ef}^{E2}(E_e) = \sigma_{ef}^{\exp} - \sigma_{ef}^{E1}. \quad (24)$$

The cross section σ_{ef}^{E1} was calculated in accordance with Eq. (3), and the photofission cross sections corresponding to $E1$ photoabsorption were taken from Ref. 42; the virtual-photon spectra were calculated by the DWBA.

Analysis of the electrofission cross-section curve shown in Fig. 20 made it possible to determine $\sigma_{\gamma f}^{E2}$ (Fig. 21). Similar results were obtained for ^{234}U and ^{236}U. Table I gives data on the properties of the isoscalar quadrupole resonance obtained from reactions with α particles[71] and ^{6}Li nuclei,[72] and also average data on the fissilities of these nuclei, taken from Ref. 50. Note the discrepancy between the fissility data obtained in experiments with electrons and with strongly interacting particles. It was asserted in Refs. 69 and 70 that in the case of $E2$ excitation the fissility is higher than in the case of $E1$ (see Table I).

To confirm their experimental data, Arruda Neto *et al.* made additional experiments at Stanford,[65] in which they measured coincidences of scattered electrons with fission fragments and, thus, determined the nuclear-excitation energy. The measurements were made with incident electrons of energies 80.1 and 117.7 MeV at scattering angles 40° and emission angles 0–180° of the fragments (Fig. 22). The results of these measurements confirmed the data obtained earlier for ^{238}U (Fig. 23).[70]

However, subsequently published preliminary results of new measurements made at Stanford by other authors[74] using a similar method (with detection of coincidences between fission fragments and scattered electrons) gave a probability near 16% for decay of the isoscalar quardrupole resonance for the ^{238}U nucleus. It should be mentioned that the authors of Ref. 74 do not yet regard their data as definitive.

Recently published data[75] contradict the results of the Brazilian group. As can be seen in Fig. 24, which is taken from Ref. 75, the results of this work give no grounds for drawing a conclusion about the contribution of the $E2$ resonance to ^{238}U photo- and electrofission. Thus, the problem of the accuracy of the measurements of the absolute values of σ_{ef} remains the main problem, and new experiments are needed to study the contribution of the $E2$ excitation to electrofission.

It should be noted that an increase in the fissility of the ^{238}U nucleus in the region of the $E2$ resonance was observed in reactions induced by μ mesons.[76] In case this the nucleus is excited mainly by a muon transition between the $3p$ and $1s$ shells, the energy of the photon captured by the nucleus in the nonradiative process being 9.44 MeV. The presence of the muon in a nuclear orbit strongly changes the fission barrier, and therefore the data obtained in electron and muon reactions can be compared only qualitatively. It is interesting to note that the statistical model gives a different dependence of the ratio of the neutron and fission widths for $E1$ and $E2$ excitations on the excitation energy.[76,50]

The data[77] on the electrofission cross sections at energies from 20 to 120 MeV give information about the integrated cross sections $\int \sigma_{\gamma f}^{E1}\, dE_\gamma$ and $\int \sigma_{\gamma f}^{E2}\, dE_\gamma$ (Fig. 25). In estimating the integrated cross sections, it was assumed that the $E2$ resonances are concentrated at $E_\gamma \sim 9$ and 22 MeV.

The electrofission cross sections of ^{232}Th, ^{233}U, ^{235}U, ^{238}U, ^{237}Np, ^{239}Pu, ^{241}Am, and ^{243}Am at energies above 100 MeV were measured in Refs. 78 and 79. Data for some of these nuclei are given in Fig. 26. It can be seen that for all the transuranium nuclei the cross sections are equal to within the errors.

Comparing the results of the measurements of σ_{ef} for ^{238}U obtained by different authors, we conclude (Fig. 27) that is the data of Ref. 7, obtained in 1969, are ignored, the uncertainty in the absolute value of the cross sections is about $\pm$ 10%, which is much better than for the investigations made using the bremsstrahlung beam (see Fig. 9).

TABLE I. Data on the isoscalar quadrupole resonance obtained in different nuclear reactions for nuclei with $Z \geqslant 92$.

Reaction	Nucleus	E_{res}, MeV	ΔE, MeV	$D_f^* = \frac{\Gamma_f}{\Gamma_{tot}}$	Литература
(e, f)	^{234}U	8.2±0.4	4,8±1,0	0.70±0.15	[65]
(e, f)	^{236}U	8,9±0,4	4,7±1,0	0,60±0.10	[69]
(e, f)	^{238}U	8.3±0,4	5,0±1.0	0,40±0.10	[70]
$(e, e'f)$	^{238}U	9,5		0.16	[74]
$(\alpha, \alpha' f)$	^{238}U	11	4±0,5	0,10	[71]
$(^6\text{Li}, \text{Li}f)$	^{238}U	10,5	7	0,20	[72]
$(\alpha, \alpha' f)$	^{238}U	10,6	2.2±0,2	0.25±0.10	[72]
(e, f)	^{238}U	No resonance			[75]

* Средняя делимость $\overline{D}_f = 0{,}41$, 0,34, 0,20 для ядер ^{234}U, ^{236}U и ^{238}U соответственно [50].

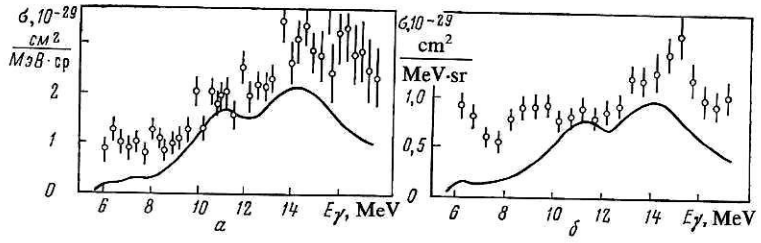

FIG. 22. Spectra of coincidences of the products of the ^{238}U$(e, e'f)$ reaction measured at scattering angle $\theta_e = 40°$ and electron energy $E_e = 80.1$ MeV (a) and $E_e = 117.7$ MeV (b). The continuous curves show the contribution of the $E1$ giant resonance; E_γ is the energy transferred to the nucleus by the virtual photon.

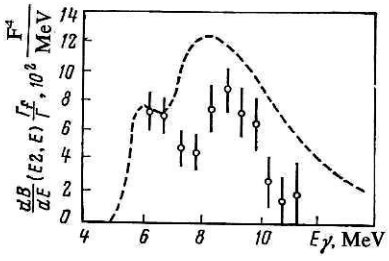

FIG. 23. Photofission cross sections $\sigma_{\gamma f}^{E2}$ obtained from the experiments of Ref. 65 for ^{238}U (e, f the broken curve, and $e, e'f$ the points).

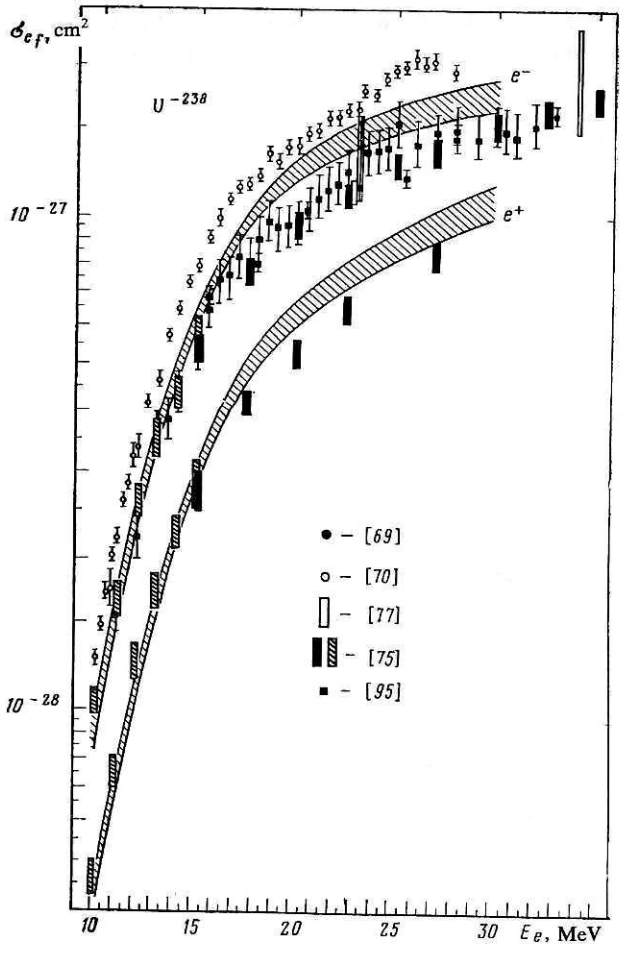

FIG. 24. Electrofission cross sections measured in different studies for the ^{238}U nucleus. (References are indicated in square brackets.)

The results of the calculation of σ_{ef} shown in Fig. 28 by the continuous curves were obtained using Eq. (3). Separately shown are the contributions of the $E1$ and $E2$ resonances (in accordance with the cross sections of Refs. 42 and 70, respectively), and also the contributions from quasideuteron photoabsorption $[\sigma_{\gamma f}^{qd} = 10(NZ/A)\sigma_{\gamma d} e^{-60E_f}$ (see Fig. 10)] and pion photoproduction on nucleons of the nucleus $\sigma_{\gamma f}^{\pi} = A\bar{\sigma}_{\gamma p}$ (see Fig. 13). The spectra $N_{\lambda L}$ were calculated in accordance with (7) in the PWBA without allowance for the nuclear size. In the calculation it was assumed that the quasideuteron interaction and the photoproduction are due to $E1$ absorption. Therefore, the error in the calculations should not exceed 15%.

The calculated curves give a basically good description of the relative dependence of the experimental data, but in absolute magnitude the experimental points lie somewhat higher than the calculated curves at all energies from 100 to 1000 MeV. This can be regarded as an indication that the photofission cross sections used in the calculation are somewhat too small. For comparison, in Fig. 28 we show calculated curves in which $\sigma_{\gamma f}^{\pi} = A\bar{\sigma}_{\gamma p}$ were replaced by values 1.5 times larger. However, the insufficient accuracy of the experimental data, as well as the ambiguity in the calculation of the virtual-photon spectra make it impossible to draw a definitive conclusion.

Calculations made with allowance for the nuclear size ($R = R_0 A^{1/3}$) in Ref. 28 showed that the introduction of a form factor merely increases the discrepancy between theory and experiment. Figure 29 shows the calculated curves for the nucleus ^{237}Np (for the remaining nuclei, they are basically similar), in which σ_{ef}^{E1} and σ_{ef}^{E2} were obtained by integration over the spectra N_{E1} and N_{E2} calculated in accordance with (11) and (12). The spectra corresponding to the quasi-

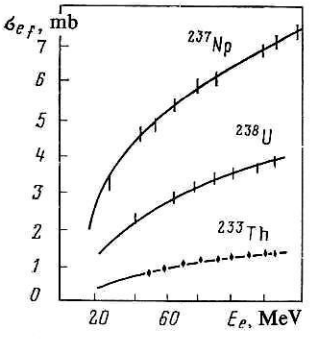

FIG. 25. Electrofission cross sections in accordance with the data of Ref. 77.

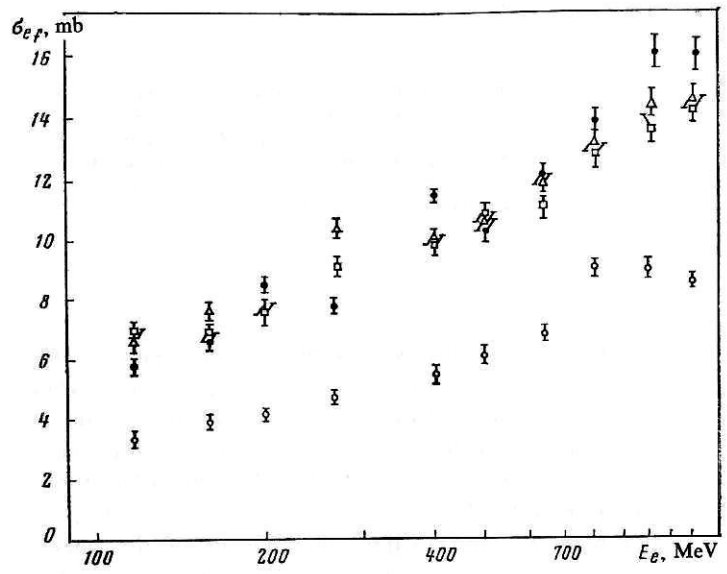

FIG. 26. Electrofission cross sections of the transuranium nuclei ^{237}Np (open squares), ^{239}Pu (open triangles), ^{243}Am (black circles), and ^{238}U (open circles).[28]

deuteron mechanism of photoabsorption (N_{E1}) and photoproduction (N_{E2}) were taken without allowance for a form factor in this case too.

In Ref. 28, an attempt was made to explain at least partly the discrepancy between the theory and experiment as due to the contribution from quasielectric scattering. If it is assumed that the energy E_{QE} transferred to the proton in the quasielectric scattering is used entirely on excitation of the nucleus, then beginning with energies $E_{QE} > B_f$ is the fission barrier, the nucleus can fission and beginning with energies $E_{QE} \geqslant 8$ MeV the fission probability becomes appreciable. Therefore, it is possible to estimate an upper limit on the electrofission cross section due to quasielectric scattering:

$$\sigma_{ef\,\max}^{QE} = 2\pi Z \int_{\theta_{\min}}^{\pi} \left(\frac{d\sigma}{d\Omega}\right)_R \sin\theta\, d\theta, \qquad (25)$$

where Z is the charge of the nucleus, $(d\sigma/d\Omega)_R$ is the cross section of electron scattering on hydrogen, θ is the scattering angle, $\theta_{\min}$ is the angle determined from the condition $q^2 = 2E_{QE}/m_p$, where $E_{QE} = 8$ MeV, and m_p is the nucleon mass. The cross section of quasielastic electron–neutron scattering is small and can be ignored. The estimates of σ_{ef}^{QE} in accordance with (25) give a value of about 1 mb for the region $E_e = 100$–1000 MeV. However, this is a strong overestimate, since it does not take into account the Pauli principle as in the modified quasideuteron model.[45] In contrast to free nucleons, nucleons in a nucleus cannot acquire an energy below the Fermi limit, and therefore E_{QE} should be not 8 MeV but about 35 MeV, which decreases σ_{ef}^{QE} by about four times. Thus the question of the electrofission cross sections

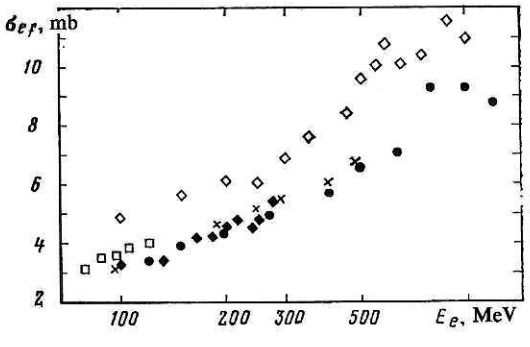

FIG. 27. Comparison of data on ^{238}U electrofission cross sections obtained in Ref. 6 (crosses), Ref. 7 (open diamonds), Ref. 28 (black circles), Ref. 77 (open squares), and Ref. 78 (black diamonds) at intermediate energies.

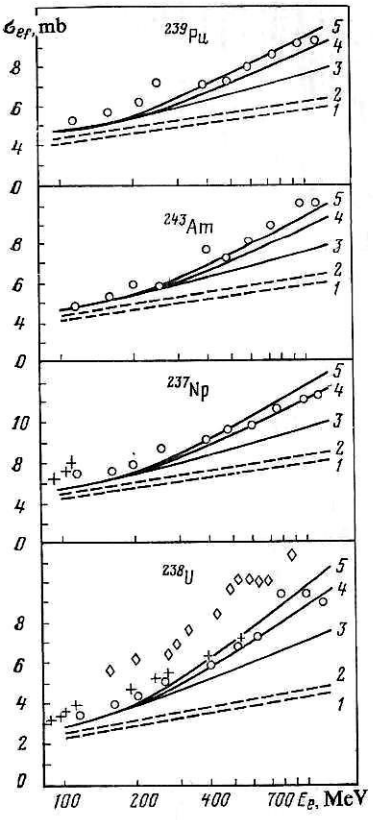

FIG. 28. Comparison of experimental σ_{ef} values for ^{238}U, ^{237}Np, ^{239}Pu, and ^{243}Am with calculations: 1) $\sigma_1 = \sigma_{ef}^{E1}$; 2) $\sigma_2 = \sigma_1 + \sigma_{ef}^{E2}$; 3) $\sigma_3 = \sigma_2 + \sigma_{ef}^{qd}$; 4) $\sigma_4 = \sigma_3 + \sigma_{ef}^{\pi}$; 5) $\sigma_5 = \sigma_4 + 0.5\sigma_{ef}^{\pi}$.

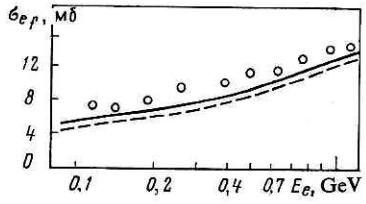

FIG. 29. The ^{237}Np electrofission cross section calculated with allowance for the nuclear structure (broken curve) and compared with experimental data (open circles).[28] The continuous curve is the calculation without allowance for the form factor (the same as curve 4 in Fig. 28).

at intermediate energies remains open from both the experimental and the theoretical point of view.

7. PHOTO- AND ELECTROFISSION CROSS SECTIONS OF NUCLEI WITH Z⩽83 NEAR THE THRESHOLD

Study of the fission near the threshold gives information about the barrier, the density of levels at the saddle point, and the photon–nucleus interaction mechanism. For nuclei with $Z \leqslant 83$, data on fission near the threshold are very sparse. This is mainly due to the very small cross section in this region of energies. Thus, for bismuth in the interval of $E_{\gamma\max}$ from 140 to 40 MeV the photofission yield decreases by seven orders of magnitude, as can be seen in Fig. 30.

Advance into the region of small cross sections was made possible by solid-state track detectors. Data have been obtained for the nuclei of gold,[80] bismuth,[81] lead isotopes,[82] and tungsten.[83]

In the overwhelming majority of cases, the near-threshold fission experiments were made directly in the electron beam, since in this case the highest (compared with photons) density of events is achieved. Figure 31 shows the electrofission cross sections of the lead isotopes as functions of the electron energy.[82] Note the presence of the resonances in the cross section at $E_{\text{exc}} \sim 35$ MeV for the ^{206}Pb and ^{207}Pb nuclei but the absence of such a resonance of ^{208}Pb. The nature of these resonances cannot be explained in the framework of the existing models, and therefore further experimental investigations are needed in this direction. Analysis of the experimental data on the basis of the evaporation model give fission barriers of 26.0 ± 0.5, 26.2 ± 0.5, and 27.7 ± 0.5 MeV for the nuclei ^{206}Pb, ^{207}Pb, and ^{208}Pb, respectively.

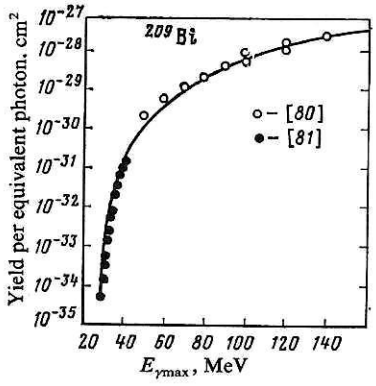

FIG. 30 Photofission yield for the bismuth nucleus (references are indicated in square brackets).

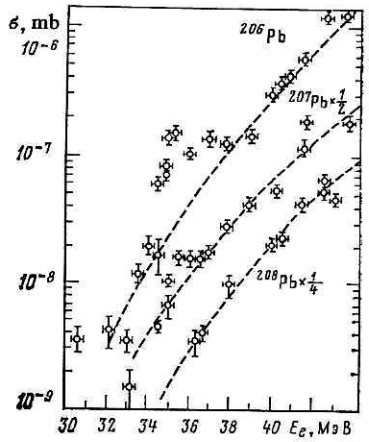

FIG. 31. Electrofission cross sections for ^{206}Pb, ^{207}Pb, and ^{208}Pb.[82]

It should be noted that the use of photons or electrons as bombarding particles has, as noted above, definite advantages in the study of below-barrier fission over heavy particles, which introduce a large orbital angular momentum into the nucleus.

8. ANGULAR DISTRIBUTIONS OF THE FRAGMENTS OF PHOTO- AND ELECTROFISSION

The angular distributions of the fragments of photo- and electrofission are anisotropic at low energies, when the number of fission channels is limited and the probability of emission of the fragments at a definite angle is determined by the orbital angular momentum introduced into the nucleus. Figure 32 gives the results of Ref. 84 at $E_e = 6$ MeV, which show that in the case of ^{236}U electrofission the contribution of the quadrupole component is appreciably higher than in photofission. The dependence of the coefficient $C(E2)$ in the expansion of the angular-distribution function

$$F(\theta) = a + b \sin^2\theta + C \sin^2 2\theta \qquad (26)$$

is shown in Fig. 33. This coefficient characterizes the fraction of the quadruple excitations in the nuclei. Note the good agreement between the DWBA calculations and the experimental data: $C^{\text{DWBA}}/C^{\text{exp}} = 0.94 \pm 0.14$ for ^{236}U and 1.07 ± 0.04 for ^{238}U.

Estimates of the contribution of the quadrupole (isoscalar) component to the electrofission cross section of transuranium nuclei on the basis of an analysis of the angular distributions were made in Ref. 83. It was shown that for ^{232}Th this contribution remains appreciable (about 10%) in the re-

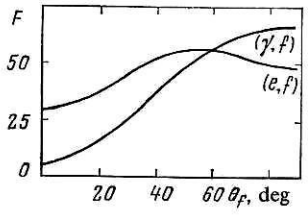

FIG. 32. Angular distribution of the fragments of photo- and electrofission of ^{236}U at $E_e = 6$ MeV.[84]

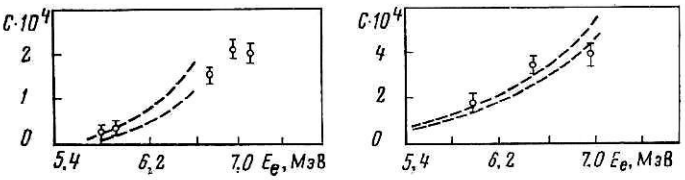

FIG. 33. The coefficient C in the angular distribution $F(\theta)$ as a function of the electron energy for the ^{236}U nucleus.[69]

gion of energies 5.5–7.0 MeV, which lie appreciably lower than the maximum of the $E2$ resonance.

At energies above 12 MeV up to 2 GeV the angular distributions of the fragments of photo- and electrofission of heavy nuclei ($Z \geqslant 90$) are isotropic to within the errors of the measurements (about 2–3%), but for moderately heavy nuclei at intermediate energies there is a weak anisotropy due to the motion velocity of the fissioning nucleus.[85,86] If the angular distribution of the fragments in the system attached to the nucleus is isotropic, then in the laboratory system it takes the form

$$\frac{d\sigma}{d\Omega} \sim 1 + 2\frac{v}{V}\cos\theta, \tag{27}$$

where V is the velocity of the fragment in the frame attached to the nucleus, and v is the velocity of the nucleus before fission.

Figure 34 shows the angular distribution of the photofission fragments of the bismuth nucleus.[86] It can be seen that there is a directionality of the forward distribution, the anisotropy coefficient being about 0.1 and weakly dependent on $E_{\gamma\max}$ in the range 1 – 1.5 GeV.

If one fragment is detected, the velocity of the fissioning nucleus is determined as an averaged quantity over many fission events. If both fragments are detected in coincidence, this velocity can be determined for each event separately. It follows from the coincidence measurements of Ref. 87 that the emission angle of the fragments is less than 180°, which indicates that the nucleus has a certain velocity before fission.

The angular distributions of the electrofission fragments of nuclei with $Z \geqslant 90$ at $E_e \geqslant 50$ MeV are, as in the case of photofission, isotropic.[88]

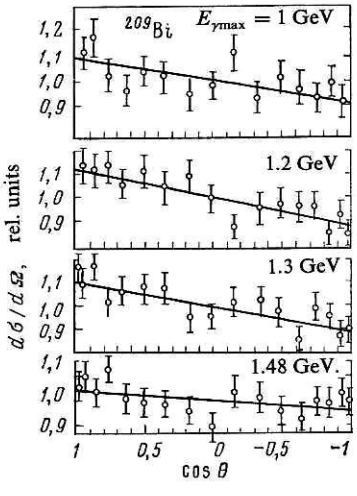

FIG. 34. Angular distribution of the photofission fragments of bismuth nuclei.[86]

9. DISTRIBUTIONS OF THE MASSES AND KINETIC ENERGIES OF THE FRAGMENTS

Study of the mass and kinetic-energy distributions of the fragments gives more detailed information about the fission mechanism. With regard to photo- and electrofission, this means above all the possibility of establishing the proportion of $E1$ and $E2$ excitations in the nuclei. The main results in this direction in the region of intermediate energies were obained by Shotter[89,90] and Aschenbach *et al.*[91] In the first investigation, the fragments were detected by semiconductor surface-barrier detectors, and in the second by dielectric track detectors, the dependence of the track diameter on the fragment mass being used. Figure 35 shows the dependence of the relative number of counts on the track diameter for ^{238}U. The resolution ΔM was about 2.5 amu. The mass distribution is characterized by a two-hump distribution, the magnitude of the dip decreasing with increasing electron energy because of the increase in the contribution to the fission of the symmetric component. Similar distributions are observed in different reactions for the majority of heavy nulei with $Z \geqslant 90$.[50]

The fragment mass distributions of electron- and photon-induced fission were compared in Refs. 89 and 90. Figure 36 shows the ratio of the yields of symmetic and asymmetric fission $Y_{\text{sym}}/Y_{\text{asym}}$, for the reactions ^{235}U$(e, e'f)$, ^{238}U$(e, e'f)$, and ^{238}U$(\gamma, \mathbf{f})$ measured in the electron-energy range E_e = 20–120 MeV. In this case, the energy of the upper limit of the bremsstrahlung spectrum, $E_{\gamma\max} = E_e - m_e$, was effectively equal to E_e. It can be seen that the contribution of the symmetric component for ^{238}U in the case of electrofission is higher than in the photofission of the same nucleus. This result was interpreted qualitatively in Ref. 89 as a manifestation of a dependence of $Y_{\text{sym}}/Y_{\text{asym}}$ on the mean excitation energy of the nucleus, which according to the obtained data must be higher in the case of electrons than for photons. Since in photofission the nucleus is excited predominantly, as was noted above, by the giant dipole resonance, the obtained data may mean that in electrofission an important

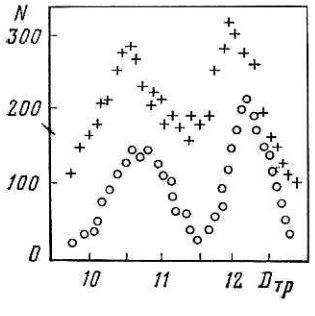

FIG. 35. Distribution of the ^{238}U electrofission fragment masses at electron energy E_e = 13 MeV (open circles) and 60 MeV (plus signs).[91]

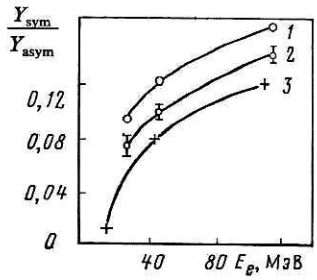

FIG. 36. Ratio of the fragment yields of symmetric and asymmetric fission from the reactions: 1) ^{235}U(e,f); 2) ^{238}U(e,f); 3) ^{238}U(γ, f) (Refs. 89 and 90).

part is played by excitations at higher energies, for example, an isovector $E2$ resonance. At the same time, it should be noted that the virtual photon spectrum falls off more rapidly with increasing energy than the bremsstrahlung spectrum (see Figs. 2–5), so that if the absorption cross sections for bremsstrahlung and virtual photons are due solely to $E1$ interaction the mean excitation energy in the first case (for irradiation by bremsstrahlung photons) must be higher. This contradicts the dependence shown in Fig. 36. Obviously, it would be very interesting not only to make the experimental data mentioned above more accurate but also to obtain similar results for a greater number of nuclei.

From Fig. 36 it can also be seen that the contribution of the symmetric component for ^{235}U is higher than for ^{238}U. This result agrees with the data obtained in other nuclear rections and confirms the well-known ideas about the part played by shell effects in the formation of the fission fragments.[50]

If we consider the distribution of the average kinetic energies ($\bar{E}_{kin}$) of the fission fragments, a difference in the data due to the type of excitation (electron or photon) is also manifested in the experiments,[90] although it lies mainly within the errors of the measurements (Fig. 37). Figure 37 shows the dependences of $\bar{E}_{kin}$ and of the distribution width $\Delta\bar{E}_{kin}$ on the mass of the heavy fragment for the nuclei ^{209}Bi, ^{232}Th, and ^{238}U, measured at $E_e = 120$ MeV, in comparison with the data obtained using a bremsstrahlung beam with $E_{\gamma max} = 600$ MeV.[90,92] It can be seen that $\bar{E}_{kin}$ for ^{238}Th and ^{238}U is 10 MeV higher in the case of electrofission than for photofission. The comparison is rather qualitative because of the large difference between E_e and $E_{\gamma max}$, but it is justified, since the main contribution at these energies is, as was noted above, made by collective excitations (giant resonances), which lie at low energies. Moreover, to a higher value of $E_{\gamma max}$ there corresponds a larger value of the average excitation energy of the nucleus and an increase in the contribution of symmetric fission. In the experiment, as in the case of the measurement of the mass distributions, the opposite dependence is observed.

The dependence of E_{kin} on the mass of the heavy fragment for ^{235}U and ^{238}U at $E_e = 30$, 50, and 115 MeV is shown in Fig. 38. The broken curve is calculated using the liquid-drop model. Thse data are obtained under the assumption that the mass distributions can be approximated

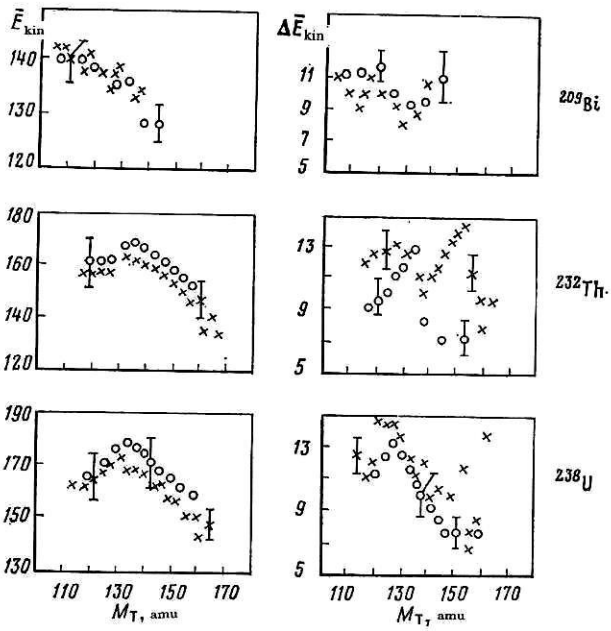

FIG. 37. Dependence of $\bar{E}_{kin}$ and $\Delta\bar{E}_{kin}$ on the heavy-fragment mass in ^{209}Bi, ^{232}Th, and ^{238}U fission. The open circles are for the (γ,f) reaction, and the crosses for the (e,f) reaction.

by two Gaussian curves corresponding to symmetric and asymmetric fission.[89]

On the basis of the few available data it can be concluded that the most interesting question is that of the mechanism that increases the contribution of the symmetric component in the electrofission of nuclei with $Z \geqslant 90$. It is as yet not possible to say whether this is a mechanism with excitation of $E2$ resonances or whether it has a different nature. For this, new experimental data are above all needed.

10. FUTURE EXPERIMENTS

The main features of photon- and electron-induced fission at intermediate energies have now been clarified. The main method used to analyze data on electrofission cross sections is still the virtual-photon method. Further progress in the study of fission will be governed by increasing accuracy of the experiments and, to no lesser degree, by the quality of the theory. The most effective ways of raising the accuracy will be to use quasimonoenergetic photons and tagged photons, and to perform correlation electrofission experiments with detection of the inelastically scattered electrons and the fission fragments.

Among the promising problems for the next years in the investigation of photo- and electrofission are the study of the total cross sections for photoaborption of real and virtual photons in nuclei.

An important direction is still the investigation of giant multipole resonances and their manifestations in the properties of the observed distributions of the fission fragments. Very important is the measurement of the mass and energy distributions of the fission fragments in a wide range of photon and electron energies.

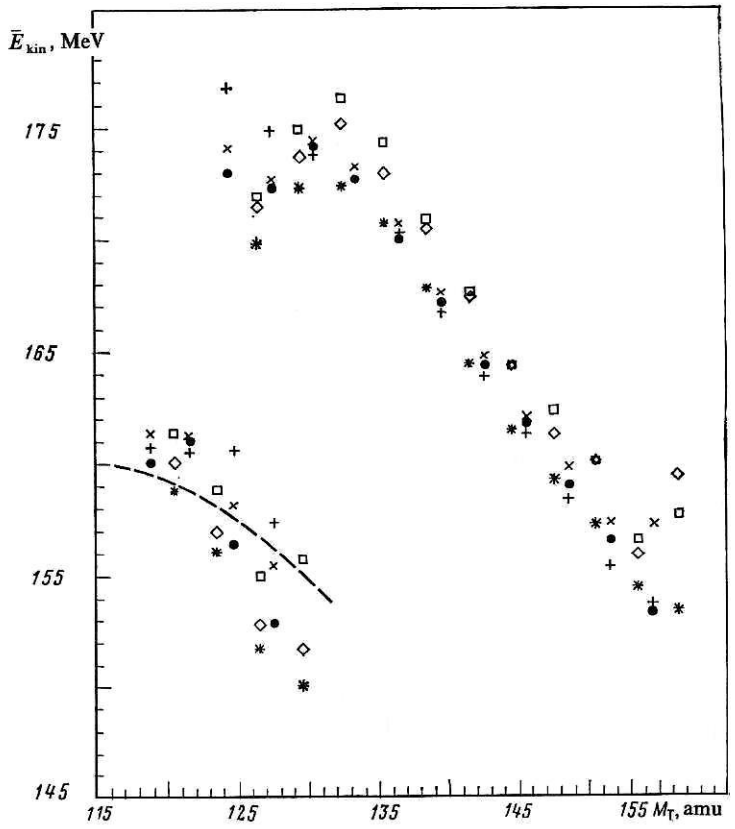

FIG. 38. Dependence of $\bar{E}_{kin}$ on the heavy-fragment mass for symmetric (at the top) and asymmetric (at the bottom) fission fragments. ^{235}U: black circles, $E_e = 30$ MeV, plus signs, 50 MeV, crosses, 115 MeV; ^{238}U: open squares, $E_e = 30$ MeV, stars, 50 MeV, open diamonds, 115 MeV.[90]

Also topical is the study of spontaneously fissioning isomers[93] in reactions induced by electrons and photons, especially at intermediate energies. At these energies, the isomer production probability depends weakly on the excitation energy, and therefore, as was noted in Ref. 94, measurement of the isomer yield can significantly extend the possibilities of the method of induced activity for the investigation of partial nuclear reactions. The isomer half-lives known in the region of the nuclei U, Np, Pu, Am, Cm, Bk differ strongly, and therefore different isotopes can be readily identified. Despite the relatively low isomer yield (10^{-4}–10^{-6}) relative to prompt fission, the background conditions are easier for the detection of delayed fragments.

The study of hypernuclei in photon- and electron-induced reactions, which has begun in recent years,[96] is of great interest.

Photofission experiments using beams of polarized photons and oriented nuclei are very promising. The information which they will yield will undoubtedly be of interest for both fission physics and the electromagnetic interactions of heavy nuclei.

[1]Proc. of the Symposium on Perspectives in Electron- and Photo-Nuclear Physics, Saclay, France, 1980, in: Nucl. Phys. **A358** (1981).
[2]B. Forkman and B. Schrøder, Phys. Scr. **5**, 105 (1972).
[3]P. V. Sorokin, in: Trudy II seminara. Élektromagnitnye vzaimodeĭstviya yader pri malykh i srednikh énergiyakh (Proc. of the Second Seminar: Electromagnetic Interactions of Nuclei at Low and Medium Energies), Nauka, Moscow (1973), p. 348.
[4]Yu. N. Ranyuk, in: Trudy III seminara. Élektromagnitnye vzaimodeĭstviya yader pri malykh i srednikh énergiyakh (Proc. of the Third Seminar: Electromagnetic Interactions of Nuclei and Low and Medium Energies), Nauka, Moscow (1976), p. 195.
[5]Yu. N. Ranyuk and P. M. Sorokin, Yad. Fiz. **5**, 531 (1967) [Sov. J. Nucl. Phys. **5**, 377 (1967)].
[6]I. A. Grishaev, V. P. Efimov, V. I. Kasilov, *et al.*, Ukr. Fiz. Zh. **14**, 1817 (1969).
[7]L. G. Moretto, R. C. Gatti, *et al.*, Phys. Rev. **179**, 1176 (1969).
[8]Yu. A. Vinogradov, V. I. Kasilov, L. E. Lazareva, *et al.*, Yad. Fiz. **24**, 686 (1976) [Sov. J. Nucl. Phys. **24**, 357 (1976)].
[9]R. H. Dalitz and D. R. Yennie, Phys. Rev. **105**, 1598 (1957).
[10]R. Bergère, H. Beil, P. Carlos, *et al.*, in: Proc. of the Fourth Seminar: Electromagnetic Interaction of Nuclei at Low and Medium Energies, Nauka, Moscow (1979), p. 200.
[11]L. Z. Dzhilavyan, V. D. Kuznetsov, N. P. Kucher, *et al.*, Preprint P-0121 [in Russian], Institute of Nuclear Theory, USSR Academy of Sciences, Moscow (1979).
[12]V. Bellini, V. Emma, D. Nigro, *et al.*, Nuovo Cimento **A55**, 183 (1980).
[13]L. I. Schiff, Phys. Rev. **83**, 252 (1951).
[14]A. S. Penfold and L. E. Leiss, Phys.Rev. **114**, 1332 (1959).
[15]B. C. Cook, Nucl. Instrum. Methods **24**, 256 (1963).
[16]D. M. Crawford, R. Koch, and H. H. Thies, Nucl. Instrum. Methods **109**, 573 (1973).
[17]K. Tesch, Nucl. Instrum. Methods **95**, 245 (1971).
[18]W. C. Barber, Nucl. Phys. **18**, 575 (1960).
[19]R. Rodenberg, Z. Phys. **166**, 439 (1962).
[20]B. B. Sinna and J. Goldemberg, Lett. Nuovo Cimento **5**, 37 (1972).
[21]W. W. Gargaro and D. S. Onley, Phys. Rev. C **4**, 1032 (1971).
[22]C. W. Sotovargas, D. S. Onley, and L. E. Wright, Nucl. Phys. **A288**, 45 (1977).
[23]E. Volynec, C. Mascati, *et al.*, Nucl. Phys. **A244**, 205 (1975).
[24]W. C. Barber, Phys. Rev. **111**, 1642 (1958).
[25]A. C. Shotter, J. Phys. G **5**, 371 (1979).
[26]R.H. Helm, Phys. Rev. **104**, 1466 (1956).
[27]M. Rosen, R. Raphael, and H. Uberall, Phys. Rev. **164**, 927 (1967).
[28]V. L. Kuznetsov, V. G. Nedorezov, N. V. Nikitina, *et al.*, Nucl. Phys. **A381**, 472 (1982).
[29]H. A. Bethe and R. E. Peierls, Proc. R. Soc. London, Ser. A **148**, 136 (1935).
[30]T. Metasiri, Nucl. Phys. **A158**, 433 (1970).
[31]Y. Wakuta, M. Sonoda, A. Katase, *et al.*, J. Phys. Soc. Jpn. **26** 852 (1969); **31**, 12 (1972).
[32]F. Carbonara, H. G. de Carvalho, R. Rinzivillo, *et al.*, Nucl. Phys. **73**,

385 (1965).
[33]J. Gindler and R. B. Duffield, Phys. Rev. **94**, 759 (1954).
[34]P. S. Moretto, R. P. Gatti, *et al.*, Phys. Rev. **179**, 1176 (1969).
[35]J. A. Jungerman and H. M. Steiner, Phys. Rev. **106**, 585 (1957).
[36]G. A. Vartapetyan, N. A. Demekhina, V. I. Kasilov, *et al.*, Yad Fiz. **14**, 65 (1971) [Sov. J. Nucl. Phys. **14**, 37 (1972)].
[37]V. I. Kasilov, Yu. N. Ranyuk, and P. V. Sorokin, Yad. Fiz. **11**, 1324 (1970) [Sov. J. Nucl. Phys. **11**, 736 (1970)].
[38]H. J. De Carvalho, G. Cortini, *et al.*, Nuovo Cimento **19**, 187 (1961).
[39]E. V. Minarik and V. A. Novikov, Zh. Eksp. Teor. Fiz. **32**, 241 (1957) [Sov. Phys. JETP **5**, 253 (1957)].
[40]B. M. Aleksandrov, A. S. Krivokhatskiĭ, V. L. Kuznetsov, *et al.*, Yad. Fiz. **28**, 1165 (1978) [Sov. J. Nucl. Phys. **28**, 600 (1978)].
[41]H. J. De Carvalho, C. B. Martins, *et al.*, Lett. Nuovo Cimento **14**, 615 (1975).
[42]A. Veyssière, H. Beil, R. Bergère, *et al.*, Nucl. Phys. **A199**, 45 (1973).
[43]G. M. Gurevich, L. E. Lazareva, *et al.*, Nucl. Phys. **A273**, 326 (1976).
[44]J. M. Eisenberg and W. Greiner, Nuclear Theory, Vol. 1, Nuclear Models, North-Holland, Amsterdam (1970) [Russian translation published by Atomizdat, Moscow (1975)].
[45]J. S. Levinger, Phys. Lett. **B82**, 181 (1979).
[46]O. A. P. Tavares, J. D. Pinheiro, *et al.*, Lett. Nuovo Cimento **27**, 358 (1980).
[47]I. L. Smith, J. Garvey, J. G. Rutherglen, *et al.*, Nucl. Phys. **B1**, 483 (1967).
[48]F. Partovi, Ann. Phys. (N. Y.) **27**, 79 (1964).
[49]T. A. Armstrong, W. R. Hogg, G. M. Levis, *et al.*, Phys. Rev. D **5**, 445 (1972).
[50]R. Vanderbosh and J. B. Huizenga, Nuclear Fission, Academic Press, New York (1973).
[51]V. S. Barashenkov, V. G. Zheregi, A. S. Il'inov, *et al.*, Preprint R2-7702 [in Russian], JINR, Dubna (1974).
[52]V. S. Barashenkov and V. D. Toneev, Vzaimodeĭstvie vysokoénergeticheskikh chastits i yader s atomnymi yadrami (Interaction of High Energy Particles and Nuclei with Nuclei), Atomizdat, Moscow (1972), p. 167.
[53]V. G. Vlasenko, V. A. Golshteĭn, *et al.*, Yad Fiz. **23**, 504 (1976) [Sov. J. Nucl. Phys. **23**, 265 (1976)].
[54]A. I. Lebedev, Vopr. Atomn. Nauki Tekh., Ser. Obshch. Yad. Fiz. No. 1 (1). Khar'kov Physico-Technical Institute (1978), p. 33.
[55]J. R. Nix and E. Sassi, Nucl. Phys. **81**, 61 (1960).
[56]L. N. Andronenko, L. A. Baĭshnene, *et al.*, Pis'ma Zh. Eksp. Teor. Fiz. **24**, 619 (1976) [JETP Lett. **24**, 573 (1976)].
[57]A. V. Gann, T. S. Nazarova, V. I. Noga, *et al.*, Yad. Fiz. **30**, 876 (1979) [Sov. J. Nucl. Phys. **30**, 453 (1979)].
[58]T. Metasiri and S. A. Johansson, Nucl. Phys. **A167**, 97 (1971).
[59]V. Emma, S. Lo Nigro, *et al.*, Lett. Nuovo Cimento **2**, 271 (1971).
[60]A. V. Mitrofanova, Yu. N. Ranyuk, and P. V. Sorokin, Yad. Fiz. **6**, 703 (1967) [Sov. J. Nucl. Phys. **6**, 512 (1967)].
[61]B. D.Pate and J. Peter, Nucl. Phys. **A173**, 320 (1971).
[62]F. M. Kiely, B. D. Pate, *et al.*, Z. Phys. **A279**, 331 (1976).
[63]I. C. Nascimento, E. Volynec, *et al.*, Nucl. Phys. **A246**, 210 (1975).
[64]U. Kneissl, C. Kuhl, *et al.*, Nucl. Phys. **A256**, 11 (1976).
[65]E. Volynec, Preprint IFUSP/271, Inst. de Fizica, Sao Paulo, Brazil (1981).
[66]U. Kneissl, G. Kuhl, *et al.*, Phys. Lett. **49B**, 440 (1974).
[67]D. F. Herring, I. C. Nascimento, *et al.*, Phys. Rev. **139**, 562 (1965).
[68]G. Kuh. U. Kneissl, *et al.*, Nucl. Phys. **A195**, 139, 559 (1972).
[69]J. D. T. Arruda Neto, S. B. Herdade, *et al.*, Phys. Rev. C **14**, 1499 (1976).
[70]J. D. T. Arruda Neto and B. L. Berman, Nucl. Phys. **A349**, 483 (1980).
[71]J. Van der Plicht, M. N. Haraken, *et al.*, Phys. Rev. Lett. **39**, 1188 (1977).
[72]F. E. Bertrand, J. R. Beene, C. E. Bemis, *et al.*, Phys. Lett. **99B**, 213 (1981).
[73]A. C. Shotter *et al.*, Phys. Rev. Lett. **43**, 569 (1979).
[74]K. Vad Bibber, P. Countryman *et al.*, Lect. Notes Phys. **158**, 278 (1982).
[75]H. Stoehner, R. D. Fischer, J. Drezler, *et al.*, Nucl. Phys. **A378**, 237 (1982).
[76]A. H. Blin and C. Wolschin, Phys. Lett. **112B**, 2 (1982).
[77]A. C. Shotter *et al.*, Nucl. Phys. **A290**, 55 (1977).
[78]V. L. Kuznetsov, V. G. Nedorezov, N. V. Nikitina, *et al.*, Ukr. Fiz. Zh. **26**, 113 (1981).
[79]V. L. Kuznetsov, V. G. Nedorezov, N. V. Nikitina *et al.*, Yad. Fiz. **30**, 1515 (1979) [Sov. J. Nucl. Phys. **30**, 785 (1979)].
[80]Yu. N. Ranyuk, P. V. Sorokin, and V. M. Sanin, Ukr. Fiz. Zh. **14**, 409 (1969).
[81]D. Turck, W. Ziga, and H. G. Clerck, Phys. Lett. **49B**, 335 (1974).
[82]D. Turck *et al.*, Phys. Lett. **63B**, 283 (1976).
[83]A. Kernohan, T. E. Drake, *et al.*, Phys. Rev. C **16**, 239 (1977).
[84]J. D. T. Arruda Neto, M. F. B. M. Vannucci, *et al.*, Phys. Rev. C **25**, 1689 (1982).
[85]I. Kroon and B. Forkman, Nucl. Phys. **A179**, 141 (1972).
[86]V. I. Kasilov, A. V. Mirofanova, Yu. N. Ranyuk, and P. V. Sorokin, Yad. Fiz. **15**, 406 (1972) [Sov. J. Nucl. Phys. **15**, 228 (1972)].
[87]A. A. Kotov, G. G. Semenchuk, and G. E. Solyakin, Preprint [in Russian], Leningrad Institute of Nuclear Physics (1975).
[88]J. D. T. Arruda Neto, S. B.Herdade, and I. C. Nascimento, Nucl. Phys. **A334**, 297 (1980).
[89]A. C. Shotter, J. M. Reid, J. M. Hendry, *et al.*, J. Phys. G **2**, 769 (1976).
[90]J. C. McGeorge, A. C. Shotter, D. Branford, and J. M. Reid, Nucl. Phys. **A326**, 108 (1979).
[91]J. Aschenbach, F. Fiedler, and E. Konecny, Nucl. Phys. **A260**, 287 (1976).
[92]M. Arescong, H. A. Gustafsson, *et al.*, Z. Phys. **A282**, 333 (1977).
[93]V. G. Nedorezov and S. M. Polikanov, Fiz. Elem. Chastits At. Yadra **8**, 374 (1977) [Sov. J. Part. Nucl. **8**, 154 (1977)].
[94]B. M. Aleksandrov, Yu. A. Vinogradov, V. A. Zapevalov, *et al.*, At. Energ. **2**, 154 (1974).
[95]J. Aschenbach, R. Haag, and H. Krieger, Z. Phys. **A292**, 285 (1979).
[96]V. E. Inopin, V. I. Hoga, S. A. Pashchuk, *et al.*, Vopr. Atomn. Nauki Tekh., Ser. Obshch. Yad. Fiz. No. 1 (19), Khar'kov (1982), p. 80.

Translated by Julian B. Barbour